ANTON FAGERSTRÖM

EFFECTS OF SURFACTANT ADJUVANTS ON PLANT LEAF CUTICLE BARRIER PROPERTIES

MALMÖ UNIVERSITY HEALTH AND SOCIETY DISSERTATION 2014:3

MALMÖ UNIVERSITY

EFFECTS OF SURFACTANT ADJUVANTS ON PLANT LEAF CUTICLE BARRIER PROPERTIES

Malmö University
Health and Society, Doctoral Dissertation 2014:3

Front illustration: Mattias Olsson, Clivia leaf and index finger
against a Brazilian cornfield backdrop.
ISBN 978-91-7104-576-8 (print)
ISBN 978-91-7104-575-1 (pdf)
ISSN 1653-5383
Holmbergs i Malmö AB 2014

ANTON FAGERSTRÖM

EFFECTS OF SURFACTANT ADJUVANTS ON PLANT LEAF CUTICLE BARRIER PROPERTIES

Malmö University, 2014
Faculty of Health and Society
Department of Biomedical Sciences

To my Family

"Never measure the height of a mountain until you have reached the top. Then you will see how low it was."

- Dag Hammarskjöld

CONTENTS

ABSTRACT

The focus of this project has been the mechanisms of action of surfactants as agricultural adjuvants and the physico-chemical interactions between adjuvant, carrier formulation, and leaf surface. To increase the understanding of this complex system, model systems have been evaluated in parallel to *in vitro* studies of plant leaf cuticle. Investigations on how thermodynamic, structural and rheological properties of leaf surface constituents are affected by surfactant absorption and hydration have been central. The main techniques employed in the project are: Environmental Scanning Electron Microscopy, Differential Scanning Calorimetry, Optical Phase Contrast Microscopy with Temperature Resolution, Quartz Crystal Microbalance with Dissipation, Small- and Wide-angle X-ray Diffraction, and Franz type diffusion cells. The effects that surfactants exert on the structure of native intact plant leaf cuticle were investigated by Small- and Wide-Angle X-ray diffraction (SWAXD). The native Clivia cuticle wax is heterogeneous and contains both crystalline and amorphous domains. The wax has a broad melting interval between 40 and 80°C which comprises a crystalline transition from orthorhombic to hexagonal sub-cell. This transition is facilitated by addition of surfactants. Both intact cuticle and extracted wax also possess lamellar long range order. *Clivia* is an appropriate model plant since it is related to, and has similar leaf characteristics as, some of the most important crop plants, wheat and barley. It is easy to cultivate indoors, and the leaves are wide enough to be evaluated *in vitro* through diffusion cell experiments. The barrier is very tough; if it works on *Clivia* it most probably will work in the field as well. The model of plant leaf intracuticular wax can be used to estimate formulations effects on the cuticle structure. A model was based on a leaf wax extract and comprised 1-docosanol ($C_{22}H_{45}OH$) and dotriacontane ($C_{32}H_{66}$). The thermotropic phase behaviour of the model was investigated, and the structure of individual phases in the model wax - water system was determined. The thermotropic transi-

tions of the model wax fit in the window of the extracted leaf waxes, but the model wax would benefit from further development, striving for a more amorphous system. The effects of surfactants on the phase behaviour and the rheological characteristics of the model wax were quantified. This was done to address the current lack of understanding of how surfactants affect the barrier properties of plant leaf cuticles on a molecular level. The model wax used is crystalline at ambient conditions, yet it is clearly softened by the surfactants. The softness of the wax film increased in irreversible steps after surfactant exposure and of the two surfactants used, $C_{10}EO_7$ has a stronger fluidizing effect than $C_8G_{1.6}$. Intracuticular waxes (IW) comprise both crystalline and amorphous domains. Surfactants mainly exercise their fluidizing effects in amorphous regions. A mechanism is suggested to explain the fluidizing effects seen on a largely crystalline model wax. It is proposed that surfactants may enter the crevices in between crystalline domains to establish an expanded continuous amorphous network. Surfactants allow higher amounts of active ingredients in solution, available for penetration. Commercial products (normally concentrates) may contain such high amounts of active ingredient that complete solubilisation is never reached, even after dilution. Crystalline active ingredients cannot enter the cuticle and may lead to an unnecessary environmental burden when dislocated from the leaf. The rate of active ingredient leaf uptake may be increased by an appropriate surfactant. Surfactants increase the flux of active ingredients over the cuticle barrier by increasing the diffusion coefficient inside the cuticle. Based on Fick's first law, an algorithm that accommodates changes in boundary conditions and takes partition into account was developed. It thereby provides a more accurate method, compared to the standard equations normally used for calculating solute diffusion coefficients in membranes. The same quantitative increase in both flux (J_i) and diffusion coefficient (D_i) was observed with surfactants present, while the cuticle-water partition coefficient ($\lg K_{cw}$) remained unchanged. Evaluation tools have been developed by the establishment of QCM-D and membrane diffusion protocols, and the investigations on model wax. These tools can facilitate the determination of desired properties of new and better adjuvants in agriculture. Subsequently, it may contribute to a more cost-efficient and environmentally friendly usage of pesticides in foliar spray applications. The wider aim of this project was to contribute to a more efficient and optimized pesticide application through investigation of the cuticle and its interplay with surfactant solutions.

POPULÄRVETENSKAPLIG SAMMANFATTNING

I avhandlingen undersöks växelverkan mellan det yttersta lagret på växters blad (cutikeln), aktiva substanser, och ämnen som tillsätts för att öka bekämpningsmedlens effekt, i detta fall vissa former av tensider. Barriären som hindrar upptag av främmande ämnen i växten sitter i cutikeln. Det är väl känt att tensider förstärker effekten av aktiva substanser. Kunskapen är dock liten om de mekanismer som underlättar upptaget i växtblad. Det övergripande målet i avhandlingen är att öka kunskapen om hur dessa mekanismer verkar. Att klargöra vilka effekter tensider har på cutikeln och hur dessa möjliggör ett ökat upptag av aktiva substanser. Ytterligare ett mål är att bidra till en mer ekologiskt hållbar användning och förnuftig applicering av bekämpningsmedel inom jordbrukssektorn. Det senare av dessa två mål kan uppnås genom att använda den mest effektiva tensiden för respektive bekämpningsmedel, samt det mest effektiva bekämpningsmedlet för respektive växtsort för att på så vis minimera mängden bekämpningsmedel. Men optimering kräver givetvis förståelse. Det övergripande målet har uppnåtts genom kartläggning av vad som sker i växelverkan mellan tensid, vatten och växtblad. Beståndsdelarna som upprätthåller bladets barriäregenskaper beskrivs, samt hur deras smältbeteende och strukturella egenskaper förändras då vatten tillförs och då tensider är närvarande. En ny modell av vaxbarriären i cutikeln etableras och kartläggs. Modellen används till att undersöka de mjukgörande effekterna tensider och vatten har på cutikeln. Hur tensider ordnar sig i en vattenlösning och hur ordningen förändras när vatten avdunstar beskrivs i avhandlingen. Vidare kartläggs hur tensider absorberas i cutikeln och vilka strukturer som påverkas där. Drivkraften för upptag av bekämpningsmedel i växtblad förklaras, hur tensider påverkar drivkraften och vilka egenskaper hos en blandning som påverkar upptaget utrönas. Hur tensider påverkar parametrar i barriären beskrivs också. Dessa parametrar behandlas på ett sätt som gör det möjligt att förklara

de effekter som tensider faktiskt har på distributionen av bekämpningsmedel inuti cutikeln. Slutligen så utvärderas formuleringar på intakta växtblad. Detta möjliggör kartläggning över vilka roller mättnadsgraden av bekämpningsmedel i formuleringar samt effekten av tensider på växtblads barriäregenskaper spelar i bladets upptag av bekämpningsmedel. Dessa resultat sammanfattas i en ny algoritm som gör det möjligt att förutse distributionen av bekämpningsmedel i växtblad vid en given blandning. Växter utgör basen för en klart dominerande del av världens sammantagna produktion av livsmedel och djurfoder. De är också en råvara i ett flertal industriella produkter. Då befolkningen ökar och levnadsstandarden förbättras, ökar också efterfrågan på bättre mat och förbrukningsartiklar från växtbas. För att tillgodose efterfrågan strävar producenter och odlare ständigt efter ökad avkastning. Detta uppnås genom ökade odlingsarealer, effektivare användning av befintlig odlingsmark samt skydd mot skadeangrepp på växter. Det sistnämnda kan göras med hjälp av olika bekämpningsmedel som innehåller aktiva substanser. Faktum är att en livsmedelsproduktion på dagens nivå inte hade varit möjlig utan användning av bekämpningsmedel. Dessa ämnen innebär dock risker, användningen är inte fullt optimerad och förståelsen för skeenden och processer i samband med dess användning är i vissa avseenden fortfarande bristfällig.

LIST OF PUBLICATIONS

This thesis is based on the following papers, which are cited in the text by their Roman numerals. The papers are appended in the end of the thesis.

I. Fagerström A, Runnsjö A, Kocherbitov V, Engblom J. *Plant leaf cuticle structure – effects of temperature, relative humidity, and surfactant absorption.* Manuscript.

II. Fagerström A, Kocherbitov V, Westbye P, Bergström K, Mamontova V, Engblom J. *Characterization of a plant leaf cuticle model wax, phase behaviour of model wax - water systems.* Thermochim. Acta, 571 (2013) 42– 52.

III. Fagerström A, Kocherbitov V, Westbye P, Bergström K, Arnebrant T, Engblom J. *Surfactant softening of plant leaf cuticle model wax – a Differential Scanning Calorimetry (DSC) and Quartz Crystal Microbalance with Dissipation (QCM-D) study.* J. Colloid Interface Sci., 426 (2014) 22-30.

IV. A.Fagerström A, Kocherbitov V, Ruzgas T, Westbye P, Bergström K, Engblom J. *Effects of surfactants and thermodynamic activity of model active ingredient on transport over plant leaf cuticle.* Colloids Surf. B, 103 (2013) 572– 579.

Paper I: I, JE, AR, and VK designed the study. I, AR, JE and VK performed all experiments and analysed the data. I wrote the paper with contributions from JE, VK and AR.

Paper II: I, VK, JE, PW and KB designed the study. I performed all experiments except GC-MS and analysed the data together with JE and VK. VM performed the GC-MS analysis. I wrote the paper with contributions from JE, VK, PW, KB and VM.

Paper III: I, PW, VK and JE designed the study. I performed all experiments and analysed the data together with VK, JE and PW. I wrote the paper with contributions from VK, JE, TA PW and KB.

Paper IV: I, JE, VK, KB, TR and PW designed the study. I performed all experiments and analysed the data together with JE and VK. I wrote the paper with contributions from JE, VK, KB, TR and PW.

ABBREVIATIONS AND SYMBOLS

Clivia	*Clivia Miniata* Regel
IW	intracuticular wax
EW	epicuticular wax
CM	cuticle membrane
CM-e	enzymatically isolated CM
CM-d	dermatomed CM
EWL	epicuticular wax layer
CP	cuticle proper
CL	cuticle layer
SCL	soluble cuticular lipids
AI	active ingredient
G	Gibbs energy
H	enthalpy
S	entropy
T	temperature
μ_i	chemical potential
t_e	lag-time
k_{ij}	partition coefficient
J_i	diffusion flux
D_i	diffusion coefficient
c_i	concentration
C^0	saturation concentration at a given surfactant concentration
a_i	thermodynamic activity
z	position
R	the universal gas constant
A	area
m	mass
V	volume

QCM-D	Quartz Crystal Microbalance with Dissipation
Δf	shift in frequency
n	frequency overtone number
C	mass sensitivity constant
G_f	complex dynamic modulus
G'_f	storage modulus
G''_f	loss modulus
μ_f	shear elastic modulus
η_f	shear viscosity
f_0	fundamental frequency of oscillation
Δf	change in frequency
ΔD	change in dissipation
ρ_i	density
h_i	thickness
ω	angular frequency
δ_b	viscous penetration depth of the shear wave
SWAXD	Small and Wide Angle X-ray diffraction
n	integer determined by the order given
λ	wave length of the beam
d	inter planar distance
θ	angle between normal of the incident beam and sample scattering planes
q	scattering vector
DSC	Differential Scanning Calorimetry
$\Delta H_{i,\,melt}$	heat effect
H_w^m	partial molar enthalpy of mixing of water (enthalpy of hydration)
a_w	water activity
P^{vap}	thermal power of vaporisation
P^{max}	maximal value of thermal power of vaporisation
P^{sorp}	thermal power in the sorption chamber.
PLOM	Polarized light optical microscopy
SEM	Scanning electron microscopy
HPLC	High Pressure Liquid chromatography
GC-MS	Gas Chromatography with Mass Spectrometry

INTRODUCTION

Background

With the increase in total world population [1] and the improved standard of living in many areas of the planet [1], the demand for food and fodder is steeply rising. Cultivated plants are at the low end of the production chain for the bulk of the supplied foodstuff, and plants are often the major raw material for many industrial commodities and final consumer products [2]. Growing demands have been met by increasing the land used for agriculture, sometimes in areas considered ecological sensitive, or otherwise ill-suited for agricultural production [3], and by strong efforts to increase crop yields [3]. Some increase in foodstuff production have been achieved by more efficient use of already cultivated lands, but the fact is that the current level of foodstuff supply would be impossible without the use of externally applied plant nutrients and pesticides [3]. Without pesticides crop yield loss would have been noticeably higher [4] and the overall effects would have been considerable. The environment would be negatively affected by more agriculture in ill-suited or sensitive areas in order to meet demands. With lower yields, farmers would have to sell less for more in order to break even. Consequently, foodstuff price of would go up as higher production costs would lead to higher consumer prices. Increased food costs would cause malnutrition and starvation, without external aid. Conflicts may arise due to an increased competition over the available food resources. Pesticide usage is however not without risks [5], neither is it always optimized [6, 7]. Pesticides may be applied at non-optimal weather conditions, too large amounts of pesticides are applied for the desired effect, and the role of agricultural adjuvants is regularly overlooked [7]. Furthermore, the way agricultural adjuvants effect foliar pesticide application is not fully understood [8].

The plant leaf cuticle

The vast majority of terrestrial plants are covered with a cuticle. The cuticle is the outermost skin of the plant and is the interface between the plant and its surroundings. The main function of the cuticle is to maintain the integrity of the plant by preventing leakage of nutrients and evaporation of water, and by protecting the plant from intrusion by foreign compounds and organisms **[8]**. Cuticle structure and characteristics vary between species and may differ greatly between plant organs **[8]**. The cuticle covering the leaf, stem, or fruit of the same plant individual thus may be much differentiated in terms of appearance, structure, and barrier properties. Moreover, the cuticle contains no cells, but comprises substances excreted by the epithelial cells at the plant surface, below the cuticle **[8]**.

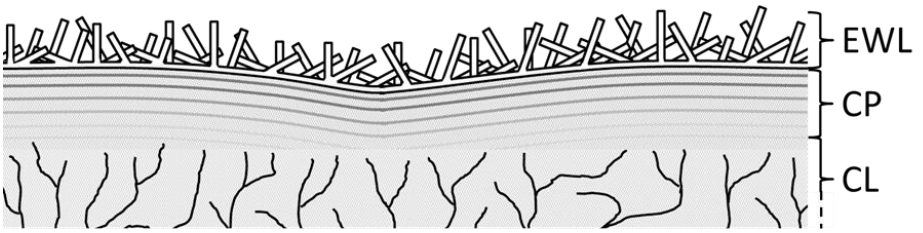

Figure 1. *Schematic transverse map of the plant leaf cuticle. Grey lines: crystalline wax domains, line network: biopolymer matrix, background: continuous amorphous domain. EWL: epicuticular wax layer, CP: cuticle proper, CL: cuticle layer. Modified after* ***[12].***

The cuticle is not a homogeneous, evenly distributed film on the surface of plant cells, but heterogeneous rather, both in the transverse and lateral directions. A plant leaf cuticle can be transversely divided into three zones **[8]** (Fig. 1). The outermost layer of the cuticle is the epicuticular wax layer (EWL). The constituents of the EWL vary between species and plant organ and consist mainly of aliphatic and aromatic nonpolar compounds, *i.e.* epicuticular waxes (EW). The waxes can be more or less ordered and usually both crystalline and amorphous domains are present **[8]**. Wax structures may protrude from the outer cuticle surface, affecting the surface characteristics of the cuticle. The intermediate zone of the cuticle, the cuticle proper (CP), is made up by intracuticular waxes (IW) embedded in a matrix of biopolymers produced by living organisms **[9]**, *i.e.* Cutin and/or Cutan **[8]**. The deepest layer of the cuticle, the cuticle layer (CL), comprises a polymer matrix composed mainly of polysaccharides and Cutin/Cutan. The layers are not discrete, but protract to some extent into each other. Cutin is a biopolymer that constitutes between 40 and

80% of the cuticle **[10]**. It is present as a polymeric network of oxygenated C_{16} and C_{18} fatty acids that are cross-liked by ester bonds **[10]**, but may also contain other compounds, like glycerol and phenolics **[11]**. The cutin may be depolymerized and dissolved by hydrolysis or other chemical methods **[10]**. The other biopolymer present in many plants, cutan, is held together by non-ester bonds and resists depolymerization **[11]**. The cutin/cutan ratio in the cuticle shows great variation with plant species and leaf development **[10]**.

Cuticle wax

In this work the terms "wax" and "waxes" are defined using the established definitions for the agrochemical and plant science research communities "-The soluble fraction obtained when CM {cuticle membranes} are extracted with suitable solvents is called soluble cuticular lipids (SCL) or cuticular waxes **[8]**. This definition differs from that used within other fields where the term "wax" often refers to an ester, or the macroscopic characteristics of a particular material **[13]**. The intra- and epicuticular waxes consist mainly of hydrophobic compounds **[14]**, and protruding structures of epicuticular wax present in many plant species may trap air at the surface of the leaves. Those are two reasons for the poor wettability observed for many plant leaf surfaces **[8]**, the so-called "Lotus effect". Moreover, the main barrier to intrusion of exogenous substances lies in the cuticle **[8]**. The waxes present in the cuticle (IW and EW) play a crucial role in maintaining the barrier properties of the whole cuticle **[8]**. Changes in the ordering and mobility of waxes can greatly affect the barrier properties of the cuticle. This may be realized by effects on the diffusion coefficient of extraneous substances in the cuticle, and by changes in the partition of such substances to the cuticle from the surrounding environment.

Role of surfactants in agricultural applications

Surfactants are widely used in agricultural applications as adjuvants to facilitate the action of another substance, the active ingredient (AI) **[8]**. Surfactants also provide other effects such as spray drift reduction, droplet size control, surface wettability, and formulation adhesion enhancement **[15, 16]**. One of the main reasons for using surfactants in agrochemical spray applications is to increase the trans-cuticle transport of systemic pesticides and plant nutrients **[8]**. Increased transport is achieved by surfactant-induced changes in the order and mobility of the cuticle constituents, leading to a less efficient barrier **[8]**.

Diffusion in the cuticle

Various pesticides and plant nutrients are commonly applied by foliage spraying, effectively locating the spray solution to the surface of the leaf **[15, 16]**. Many of the active compounds applied in this way are systemic; the desired effect is achieved after the substance has reached the interior of the plant **[15, 16]**. Hence, the substance needs to permeate the barrier of the cuticle. It is well established for more hydrophobic substances, that this penetration takes place by passive diffusion through the hydrophobic parts of the cuticle **[8]**. Amorphous wax regions are considered to be the main diffusional pathway as crystalline domains are impenetrable to AIs or surfactants **[8]**. The diffusion is driven by the difference in chemical potential of the diffusing compound (the solute) **[17, 18]**, between the plant exterior, the cuticle, and the plant interior.

Softening/Structural effects

The surfactants that are most efficient in promoting penetration of lipophilic active ingredients are so called co-penetrants **[19-21]**, *i.e.* both the surfactant and the AI enter the cuticle, ideally at the same rate **[19, 21-22]**. The surfactant affects the diffusion coefficient observed for penetrating molecules **[19, 22-23]**. This change could be related to an increase in the fluidity of the amorphous IW since the lipophilic molecules diffuse in the amorphous parts of the cuticle. It has been implicitly stated that a crystalline wax remains mostly unaffected by surfactants while the amorphous wax material does not **[24-26]**.

The scientific questions in this thesis and their relevance

It is known that surfactants may enhance the effects of pesticides and other AIs **[8]**. But the mechanisms underlying the increased leaf uptake of these substances are not fully understood **[8]**. The overall aim of this project was to increase the knowledge about the uptake mechanisms. A further goal was to contribute to a more sustainable usage and application of AIs used in agriculture. That could be achieved by optimization of surfactant-AI-plant species reciprocity, where a minimal AI amount produces the effects desired. But optimization requires knowledge. These goals were addressed by investigations of the interaction characteristics of surfactant, water, and cuticle. Tebuconazole, a systemic fungicide currently used against e.g., rust on wheat and leaf fungus, was chosen as a model AI. Leaves were retrieved from the plant *Clivia Miniata* Regel, and two surfactants, $C_{10}EO_7$ and $C_8G_{1.6}$, commonly used as adjuvants were evaluated. Surfactants interact with water, and hydration of cuticle constituents may play an important role in their mechanistic action. But

what is the aggregate structure of the surfactants in formulations? And how does this change when water evaporates? What happens when a surfactant adsorbs *on* and is absorbed *in* the cuticle? What parts of the wax matrix does it affect, and how? Can the surfactant solubilize wax from the cuticle? Paper I, by means of X-ray diffraction, systematically explores these questions by studies of intact leaf cuticle subjected to various levels of surfactant and hydration. This simulates the situation on a leaf surface after application of a surfactant water formulation. Surfactants may also absorb in the cuticle and affect the thermodynamic, structural, and rheological properties of leaf surface constituents. Which main constituents in the cuticle are responsible for the barrier properties? How are the melting characteristics and the structural properties of these substances affected by hydration and the presence of surfactants? How do the rheological properties of the cuticle constituents change when subjected to increasing levels of surfactant? Paper II and III elaborate on these questions and present data to explain the interactions between surfactant, water, and the main cuticle barrier constituents. Surfactants may affect plant leaf uptake of AIs. However, what is the driving force for AI uptake in the first place? What characteristics of the formulation influence this driving force? Does the surfactant enter the cuticle? What parameters does it affect once in the cuticle? How can these parameters be understood and contained in a way to enable a mechanistic explanation on the surfactant effects on the diffusion of AIs? These questions are answered in Paper IV where intact plant leaf cuticles were used *in vitro* to study the diffusion of a model substance.

EXPERIMENTAL TECHNIQUES AND CONSIDERATIONS

This section presents some of the techniques employed in this thesis. The major measurement techniques are described in more detail. Practical and theoretical considerations linked to each technique are briefly discussed. More in-depth information may be retrieved from Paper I-IV and references listed therein.

Diffusion cells

Diffusion cells are used to measure mass transfer across membranes. There are a number of varieties on the market but in general they fall into one of the three categories; Ussing **[27]** (static, side-by-side), Franz **[28]** (static, vertical), and Bronaugh **[29]** (flow-through, vertical). In this thesis Franz cells were used exclusively. The Franz diffusion cell is typically made of glass and consists of two parts: the lid and the body (Fig. 2). The lid has a centred cylindrical hole, which is called the donor compartment (1 ml in this study). The lid is centred on the top of the body. The body has a centred cylindrical cavity called the receptor compartment (6 ml in this study), and is surrounded by a heating jacket. A membrane is placed on top of the receptor solution, between the body and the lid of the Franz cell. The two compartments, donor and receptor, are connected and separated through the membrane. Mass transfer, *i.e.* molecular diffusion, is possible from the donor compartment to the membrane and consequently from the membrane to the receptor compartment, and in the opposite direction. The receptor compartment is continuously mixed by a magnetic stirrer.

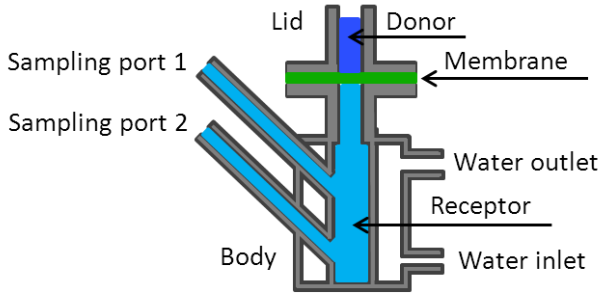

Figure 2. *Schematic drawing of a Franz diffusion cell.*

In thermodynamic terms a system can be described by its Gibbs energy, $\Delta G = \Delta H - T\Delta S$, where G is the Gibbs energy, H is the enthalpy, T is the absolute temperature, and S is the entropy of the system [17]. When temperature and pressure are constant, the Gibbs energy can be differentiated with respect to the number of molecules of a certain compound that is present in the system to give the chemical potential (μ_i) of that compound in the system [17]. At phase equilibrium, the chemical potential of component i is equal in all phases [17]. If the system is at non-phase equilibrium, differences in the chemical potential of component i are present, and a flux of molecules from high to low chemical potential takes place. This phenomenon is called diffusion and is expressed through the diffusion coefficient (D_i) [17]. A relatively high diffusion coefficient of a compound in a particular phase implies that this compound distributes relatively easy in that phase. Different molecular species have different solubilities in different phases (solid, liquid, or gaseous). This is sometimes expressed as the "affinity"; that a substance has high affinity for a certain phase means that it "likes" to be there **[30]**. All systems strive to minimize their free energy, and all systems eventually reach their minimum free energy. If pressure, and temperature are constant a smaller enthalpy (*H*) or larger entropy (*S*) produces a lower free energy **[17]**. If the change in Gibbs energy of transferring a molecule from one location to another is negative, and thermal motion is present, it will transfer by means of diffusion **[17]**. This means that a two-phase system, connected but very different in their characteristics (*e.g.* a hydrophobic membrane in a hydrophilic liquid) can contain very different levels of the same compound at the same chemical potential at equilibrium conditions.

This phenomenon is called partition **[31]**. A substance partitions more to the phase where the free energy for that compound is lower, but the entropic contribution to the Gibbs energy prevents complete partition as long as the substance has some solubility in other phases **[31]**. When calculating the diffusion coefficient of a compound over a membrane from flux data, the partition coefficient (k_{ij}) between donor/membrane and membrane/receptor needs to be known **[17]**. In practice the partition coefficient for the materials used in a particular diffusion experiment may be difficult to obtain and data for octanol/water (k_{ow}) may have to be used **[8]** (for hydrophobic materials), even though it is not optimal. Most often, calculations of diffusion data are based on results obtained through Franz cell diffusion experiments during steady-state flux conditions **[32]**. To achieve steady-state flux, sink-conditions should apply **[33]**, *i.e.* constant boundary conditions for the receptor and donor compartments. The chemical potential of a substance in the receptor solution should be low enough not to affect further uptake of the substance. In practice it usually translates to: the solute concentration in the receptor solution should never exceed 10% of its solubility limit in that solution **[33]**. Interpretation of diffusion data can be facilitated by analysis of the release profile **[34]**. Typical release profiles are shown in figure 3.

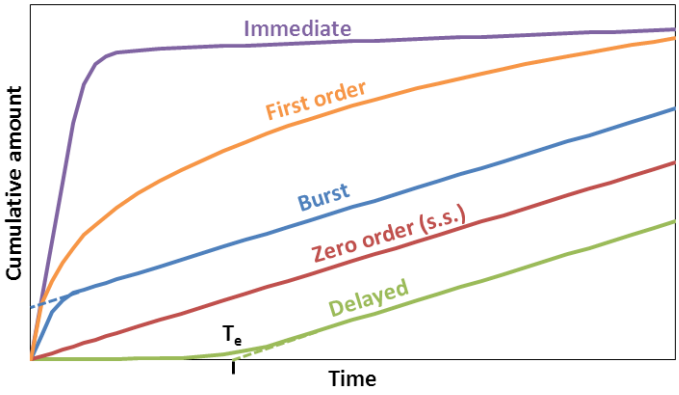

Figure 3. *Release profiles. Purple: Immediate-* ***[35]****, Orange: First order-* ***[32]****, Blue: Burst-* ***[36]****, Red: Zero order (steady state)-* ***[32, 35]****, Green: Delayed-release* ***[37]****. Curves scaled for clarity.*

Immediate release is when the membrane offers very little resistance to diffusion and equilibrium of the thermodynamic activity of the solute between the three compartments of the diffusion cell (donor, membrane, and receptor) is rapidly reached **[35]**. Burst release reflects a release, which is high in the be-

ginning, and then gradually decays towards zero order kinetics **[36]**. The opposite to burst release is referred to as the lag-time effect (or delayed release) **[36]**. The term "Fickian release" is sometimes used specifically for first order release curves, but that is somewhat misleading as all release curves follow Fick's diffusional laws **[17]**. The first part of the first order release curve can be approximated to follow zero order kinetics and pseudo steady state flux may be retrieved from this linear regime **[32]**. Zero order, or steady state, release occurs when the flux of solute from the donor to the membrane and from the membrane to the receptor compartment is constant **[32, 35]**. The activity profile of the membrane does not change as long as true steady state flux is maintained. Note however that in practice the concentrations of solute changes in the three compartments of the cell during most diffusion experiments. Delayed release is always present, even though it may not be detected due to short lag-times (T_c). It is not uncommon to see substantial lag-times in Franz cell diffusion experiments **[37]**. The delayed release arises due to a large difference in solute solubility between the donor and/or receptor compartment, and the membrane used. If the solute partitions strongly to the membrane it will take time to load the membrane before detectable amounts of solute can be released to the receptor compartment. Solute transport inside the cuticle can be described with the generalized form of Fick's first law **[17]** (Eq. 1), where the driving force (da/dz) may be separated from other effects within the membrane ($D_i c_i$).

$$J_i = -\frac{D_i}{RT} c_i \frac{\partial \mu_i}{\partial z} = -D_i c_i \frac{\partial \ln a_i}{\partial z} = -D_i c_i \frac{\partial a_i}{a_i \partial z} \qquad \text{(Eq. 1)}$$

Where: J_i is diffusion flux, D_i is the diffusion coefficient, c_i is the concentration inside the membrane, μ_i is the chemical potential, a_i is the thermodynamic activity, z is the position, R is the universal gas constant and T is the absolute temperature. The thermodynamic activity of the solute in solution is defined herein as the actual concentration of the solute divided by its solubility limit in that solution. The thermodynamic activity describes the state of a substance in a phase and is closely related to the chemical potential **[17]** (Eq. 1). The partition coefficient describes the distribution of a substance between phases. Both these notions are used in parallel to facilitate understanding of diffusion. Based on equation 1, the driving force for diffusion over a membrane like the cuticle is mainly governed by the gradient in thermodynamic activity of the solute inside the membrane (da/dz), while effects within the membrane are large-

ly reflected by the diffusion coefficient (D_i) **[17]**. The utilization of equation 1 in order to obtain diffusion coefficients from Franz diffusion cell experiments is described in detail in the results and discussion part of this thesis.

Quartz Crystal Microbalance with Dissipation

Quartz Crystal Microbalance with dissipation (QCM-D) is an experimental technique that measures the change in frequency and dissipation of an oscillating quartz crystal. The circular crystal is cut from quartz and has a conductive plating (gold) connected to electrodes. As an alternating current runs through the crystal it oscillates at a very specific frequency. Anything in contact with the oscillating sensor affects its frequency of oscillation, and material deposited on the surface of the sensor will decrease the oscillation frequency **[38]**, as described by the Sauerbrey equation (Eq. 2, **[39]**). The ability of a film deposited on top of the sensor to dissipate energy as the power input to the crystal stops, is called dissipation. A low dissipation value corresponds to a small loss of energy, indicating a more rigid film; a high dissipation value represents the opposite **[38]**.

$$\Delta m = -\frac{\Delta f}{nC} \qquad \text{(Eq. 2)}$$

Δm is the mass absorbed on the sensor, Δf is the shift in frequency, n is the frequency overtone number, and C is the mass sensitivity constant (5.72 m^2 Hz mg^{-2} at f_0 = 5 MHz). Surfactant induced effects in the cuticle material structuring can be analysed through changes in thermotropic properties of the cuticle constituents; it may also be quantified through rheological properties. In rheological terms the cuticle may be considered to be a semi-fluidic film **[25]**. The visco-elastic properties of such a film can be described by the Kelvin-Voigt model **[38, 40-42]** which is illustrated by a Newtonian damper and a Hookean elastic spring connected in parallel in figure 4 and described by equation 3.

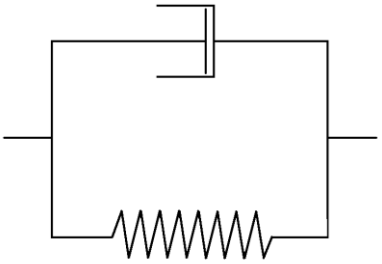

Figure 4. *The Kelvin-Voigt model.*

$$G_f = \mu_f + i\omega\eta_f = \mu_f + i2\pi f_0\eta_f = G_f' + iG_f''$$

(Eq. 3)

Where G_f is the complex dynamic modulus, G'_f (Pa) is the storage modulus, G''_f (kg/ms^2) the loss modulus, μ_f (Pa) is the shear elastic modulus, η_f (kg/ms) is the shear viscosity of the film, and f_0 (Hz) the obtained fundamental frequency of oscillation for the sensors used in this setup (4.96 MHz). The relationship of G''/G' is a measure of how fluid-like the Kelvin-Voigt film is **[38, 42]**. The higher the ratio of G''/G', the more fluid-like the film is considered to be; a value greater than 1, and a value less than 0.1 is generally considered to be fluid and stiff, respectively **[38, 42]**. QCM-D sensors (QSX 301 Gold, 100 nm, Biolin Scientific AB), were covered by a thin layer of wax by spin-coating. The wax was melted (75 °C, 5 minutes at dry conditions) in order to improve the contact between the sensor and the wax film. QCM-D experiments were modelled using the Q-tools software (Biolin Scientific AB) and the Kelvin-Voigt model (Fig. 4, Eq. 3). The experimental data (change in frequency and dissipation) are fitted by Q-tools based on equations 4 and 5 **[42, 43]**, in order to obtain film specific values for the parameters: shear viscosity, shear elastic modulus, and thickness.

$$\Delta f = -\frac{1}{2\pi\rho_q h_q}\left(h_f\rho_f\omega - 2h_f\left(\frac{\eta_b}{\delta_b}\right)^2\frac{\eta_f\omega^2}{\mu_f^2 + \omega^2\eta_f^2}\right)$$

(Eq. 4)

$$\Delta D = -\frac{1}{2\pi f\rho_q h_q}\left(2h_f\left(\frac{\eta_b}{\delta_b}\right)^2\frac{\mu_f\omega}{\mu_f^2 + \omega^2\eta_f^2}\right)$$

(Eq. 5)

Δf and ΔD are the change in frequency and dissipation, ρ_q and h_q are the density and thickness of the quartz sensor, ρ_f and h_f are the density and thickness of the film, ω is the angular frequency (ω = 2πf), η_f and μ_f are the shear viscosity and the shear elastic modulus of the film, and η_b and δ_b are the shear viscosity of the bulk liquid and the viscous penetration depth of the shear wave into this. The Kelvin-Voigt viscoelastic representation included a fluid layer and a film layer. The fundamental frequency of 4.96 MHz, and frequency and dissipation values for the 3'rd, 5'th, and 7'th overtone were used as the model input data. The fluidizing or softening effects that surfactants have on cuticle constituents can be investigated in two ways, by evaluating changes in rheological properties and in the thermotropic phase behaviour of the system. The latter is described in the DSC section of this chapter.

Small and Wide Angle X-ray Diffraction

Small and Wide Angle X-ray diffraction (SWAXD) is an experimental technique where a primary beam of X-ray photons is directed to target a sample. The beam mainly goes through the sample but some photons diffract or scatter off in directions determined by sample structure. Detectors record the diffraction intensities at small angles (SAXD) and wide angles (WAXD) compared to the direction of the incoming beam. The level of nanostructure ordering within the sample gives rise to diffraction patterns of the recorded intensities. These patterns are produced in the form of a diffraction curve, diffraction intensity versus diffraction vector q. The condition for constructive interference from successive crystallographic planes of a lattice is described by Bragg's law in equation 6 **[44]**.

$$n\lambda = 2d \sin\theta = \frac{4\pi}{q} \sin\theta \qquad \text{(Eq. 6)}$$

n is an integer determined by the order given, λ is the wave length of the beam, d is the interplanar distance, θ is the angle between the normal of the incident beam and the scattering planes of the sample, and q is the scattering vector.
SWAXD gives structural information on a sample through the analysis of Bragg peaks **[44, 45]**. In SAXD the X-ray photons are diffracted by the sample at small angles (0.1-10°) relative their trajectory of incident and in WAXD the X-ray photons are diffracted at larger angles. SAXD gives information on long range order in the length scale of 1-2 to 25 nm (or even higher for some systems) **[45]**. This makes SAXD particularly suitable to study the structure of

ordered lipid systems. SAXD gives information on whether the system is arranged in lamellar or non-lamellar (such as hexagonal, cubic) structures, as well as the dimensions of these structures. WAXD gives information on short range order on the length scale below 1 nm, and is thus usable to determine the local order of hydrocarbon chains which in turn can be used to determine whether a sample is amorphous / liquid crystalline or crystalline. The crystallographic data obtained enables the determination of the sub unit cell **[44, 46]**, such as orthorhombic (diffraction peaks at 0.42 and 0.38 nm), hexagonal (0.415 nm), triclinic (0.46 and 0.38 nm) or monoclinic (0.44, 0.41, and 0.37 nm) (Figure 5).

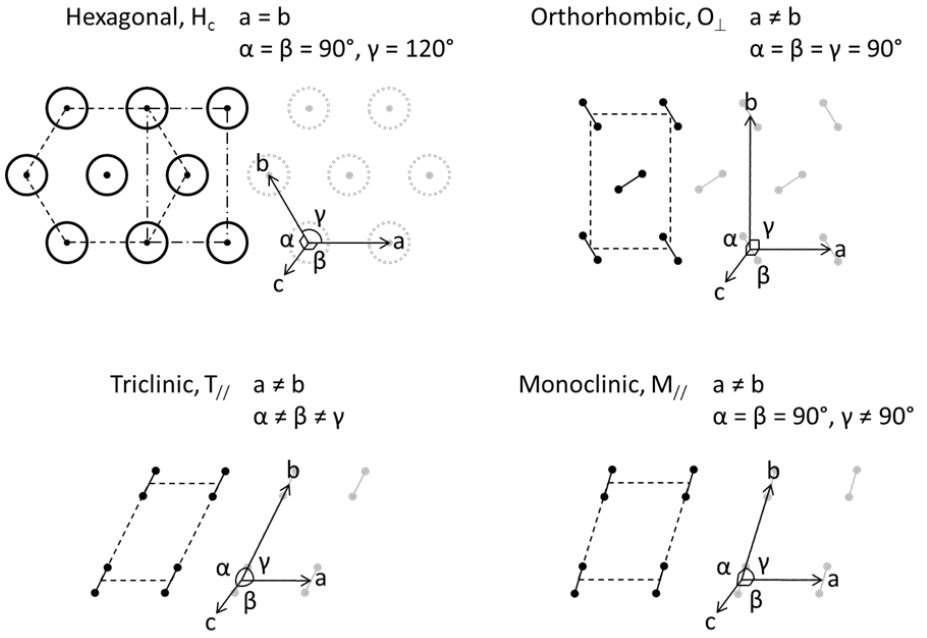

Figure 5. *Short range order. Hexagonal, Orthorhombic, Triclinic, and Monoclinic sub cells.*

In this work X-ray diffraction has been used in Paper I and II to determine the structure of both synthetic and biological waxes. Repeat distances in a lipid matrix are linked to its ability to swell upon hydration and the potential tilt-angle of the hydrocarbon chains **[47]**. In this case a greater repeat distance may correspond to a less efficiently packed phase (Paper I & II). The unit cell parameters of a lipid sub cell reflect the packing efficiency of the individual hydrocarbon chains. But it may also reflect the conformational freedom of the hydrocarbon chains in that sub-cell. A transition from a more rigid structure

(*e.g. an* orthorhombic sub-cell) to a less rigid structure (*i.e.* a rotator phase with *e.g.* a hexagonal sub-cell) is a sign of more motional freedom for the hydrocarbon chains Paper I & II). Various rotator phases have been identified, and the level of hydrocarbon chain motional freedom differs between them **[48]**. WAXD also detects lipids in an amorphous state, so it may be used to quantify the degree of crystallinity in a cuticle sample. In Paper II solid sample cells where used for SWAXD experiments on a compact Kratky camera ($\lambda(Cu\text{-}K_\alpha)$=1.542 Å), HECUS X-ray Systems, Graz, Austria. In Paper I samples were inserted into flame sealed glass capillaries (Borosilicate glass Mark-tubes, Ø = 1.5 mm, Hildenberg GmbH, Malsfeld, Germany) or a stationary solid capillary of borosilicate glass and SWAXD was performed at the MAX-lab synchrotron (MAX-lab, Lund University, Lund, Sweden) beamline 911-4.

Differential Scanning Calorimetry (DSC)

Differential Scanning Calorimetry (DSC) is an experimental technique that measures heat flow from and to a sample compared to a reference, on heating or cooling. The technique is widely used to study phase transitions and other temperature induced changes in samples of both biological and synthetic origin, including surfactants, lipids, polymers, and waxes. Endo- and exothermic effects are recorded to quantify temperature and enthalpies of transition, as well as the heat capacity of the sample. Determination of parameters in a series of samples permits the construction of binary- (T-X) and ternary phase diagrams. When energy is supplied to a system it may adapt a less ordered conformation. The ability of the system to do so may be quantified by the temperature needed for the transition to take place. Structural changes and softening of plant material may be evaluated in this way. This can be done by analysing the changes in transition temperatures of the cuticle components in the presence of a foreign compound. The inclusion of a surfactant with much lower melting point than the components of the IW may drastically decrease the melting temperature. The cause for this effect is the melting point depression that arises from a low eutectic or peritectic point between the surfactant and the wax components. Wax and surfactant are miscible in the liquid state but surfactant cannot enter the solid wax crystals **[24]**. As the entropic gain of mixing is larger for a multi-component system, the driving force for melting is increased, resulting in a lower melting temperature. In Paper II and III, DSC (DSC 1, Mettler Toledo) was used to evaluate wax/surfactant/water samples. The instrument was calibrated for heat flow and temperature using an Indium standard (T_m= 156.6 °C, ΔH= 28.45 $J \cdot g^{-1}$). A heating/cooling rate of 0.02-10 °C·min was used with start and end temperatures within the range -40 to 140

°C depending on the sample. Hermetically sealed aluminium pans (20 and 40 µl) were used for samples, with an empty pan as reference. Dry nitrogen gas (80 ml·min^{-1}) was used to purge the furnace chamber.

Isothermal Sorption Calorimetry

Heat is released or absorbed in all chemical, biological or physical processes **[47]**. Isothermal sorption calorimetry measures the heat transfer associated with the hydration of a sample. Complete thermodynamic characterization of the sample is possible with this technique as both the partial molar enthalpy of mixing, H_w^m, and the water activity, a_w, are measured continuously and simultaneously **[47]**. A completely dry sample is placed in the top chamber (sorption chamber) of the dry cell and water is injected to the bottom chamber (vaporisation chamber) of the same cell. The two steel chambers of the cell are connected through a hollow steel tube. Evaporated water diffuses through the tube and mixes with the sample. The thermal power of water vaporization and sample hydration are recorded and transformed to water activity and molar enthalpy of mixing (enthalpy of hydration) through the following two equations **[49, 50]**:

$$a_w = 1 - \frac{P^{vap}}{P^{max}} \qquad \text{(Eq. 7)}$$

$$H_w^{mix} = H_w^{vap} + H_w^{vap}\frac{P^{sorp}}{P^{vap}} \qquad \text{(Eq. 8)}$$

Where P^{vap} is the thermal power of vaporisation and P^{max} is the maximal value of thermal power of vaporisation. H_w^m is the enthalpy of vaporisation of pure water, and P^{sorp} is the thermal power in the sorption chamber. Equation 7 is actually a simplification of the more complicated equation used in the calculations **[49]**. The sorption calorimeter is equipped with two parallel cells, one for the sample and one empty reference cell; the difference between the cells is recorded. A double-twin (two chambers in each cell, and two cells) sorption calorimeter **[50]** was employed to establish the water sorption isotherm of the surfactant $C_{10}EO_7$ at 25 °C in Paper I.

Polarized light optical microscopy (PLOM)

Optical microscopy is a technique used to magnify samples and to visualize features in the µm range. Liquid crystalline phases or heterogeneously oriented crystalline domains may give rise to anisotropy in a sample **[8, 17]**. Anisotro-

py can be detected between a set of crossed polarizers. Anisotropic parts appear bright, while the background is dark. PLOM was employed in Paper I and II to investigate phase behaviour in surfactant solutions, and in native and model plant leaf cuticle wax. The technique was used in a temperature span of 20 to 120 °C.

Scanning Electron Microscopy (SEM)

Scanning electron microscopy (SEM) is a powerful technique where electrons are directed to the surface of a sample, and a range of detectors records the reflected energy, from electrons and photons of different energy. In this work detection of both secondary and back-scattered electrons was used. The technique has magnification properties down to the nm level and the Environmental type (E-SEM) enables analysis of sample features in non-vacuum as the analysis chamber may be partially filled with water vapour and the relative humidity controlled. SEM has been previously employed to study and visualize the surface of plant leaves **[8]**. In this thesis SEM was used in order to investigate the structure and to quantify the thickness of the cuticle and the underlying leaf tissue.

High Performance Liquid chromatography (HPLC-UV)

High performance liquid chromatography with UV spectrophotometric detection (HPLC-UV) was used in an assay to quantify the content of UV-active analytes in solutions. HPLC separates sample analytes in a liquid phase on a column due to the affinity of the sample analytes to that column **[51]**. The sample analyte with the smallest affinity to the column is first to pass through. HPLC was employed to analyse the content of solute in the donor and receptor solution during the Franz cell diffusion experiments in Paper IV.

Gas chromatography with Mass spectrometry (GC-MS)

Gas chromatography with Mass spectrometry (GC-MS) is a tool where a sample can be fractionated and its constituents quantified. In GC sample analytes in the gas phase are separated on a column due to their affinity for that column **[52]**. The substance with the least column affinity is eluted first from the column, and the substance with the highest column affinity exits last. The sample analyte in the column eluent is then separated according to mass in a mass spectrometer (MS) **[52]**. This technique was employed in Paper II to analyse the content of extracted plant leaf wax and to match the constituents to known substances in a database containing both aliphatic and aromatic hydrocarbons.

RESULTS AND DISCUSSION

Cuticle characterization

It is evident for the perceptive reader that what actually happens when a pesticide formulation sits on the surface of the leaf is not completely understood. The formulation contains surfactant and AI, and solvent evaporation and interaction with the cuticle is present as the droplet settles on the leaf. To bring some enhanced understanding to the complex process of cuticle/solution interaction, firstly the characteristics of the cuticle needs to be understood.

Stomata and cuticle thickness

Most terrestrial plants have stomata **[8]**. The gaseous exchange between plant leaves and the surrounding atmosphere occurs at the stomata **[8]**. It has previously been claimed that the stomata may pose a possible route for cuticle AI absorption **[8]**, and that some surfactants can wet the inner surface of the stomatal openings **[8]**. The main target here is to characterize the cuticle and the transport through the cuticle barrier and exclude stomatal uptake. Therefore, it was important to confirm that the upper (*adaxial*) surface of mature *Clivia Miniata* Regel lacks stomata. SEM was used to investigate this and micrographs of the leaf surface are shown in figure 6. Nine different leaves of three individual plants were examined and stomata where found on the lower side of the leaves but not on the upper side. From this, it can be concluded that adaxial administration of AI to Clivia does not involve the stomatal pathway. The pathway where the AI's cross the cuticle barrier by diffusion in the hydrophobic cuticle matrix **[8]** should be the dominating one. Hence, *Clivia* is a valid model for study of leaf cuticle permeability. The thickness of the barrier was determined by SEM by analysing 12 leaf segments from three individual plants, and one micrograph is shown in figure 6D. The average thickness of the cuticle was determined to be 8.5 μm. This value was used for calculating the diffusion coefficient of the AI tebuconazole in the cuticle (Eq.

1, Paper IV). The surface of the cuticle may in some species be covered with protruding wax structures **[8]**. These structures may prevent droplet spreading and wetting of the leaf surface. No such structures have been reported for *Clivia* **[8]**, and this was also confirmed by SEM (fig. 6).

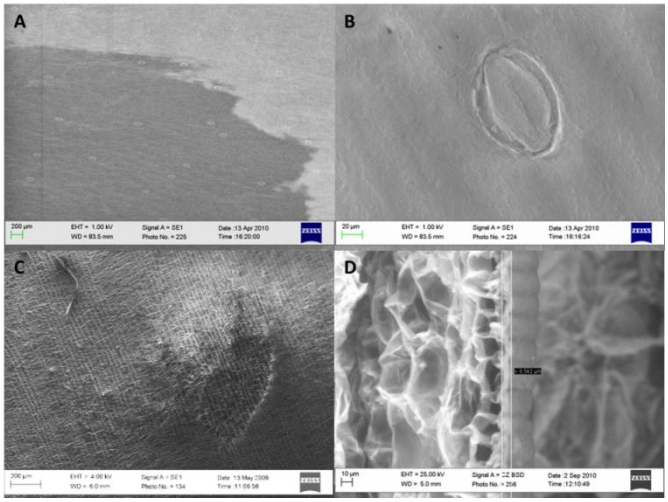

Figure 6. *SEM micrographs of the Clivia leaf surface, A: Stomata present at the lower leaf surface, B: zoom-in of a stomata, C: Lack of stomata at the upper leaf surface, D: the thickness of Clivia leaf cuticle = 8.5 µm.*

Cuticle thermotropic phase behaviour

It is established that the cuticle is the barrier that a penetrating molecule has to cross **[8]**. It is also accepted that the main obstacle in this process, *i.e.* the cuticle elements that exercise the actual barrier effect, are the cuticle waxes **[8]**. Therefore, the next step in understanding cuticle AI penetration is to map the characteristics of the cuticle and its constituents. Different methods are described in the literature for extracting plant leaf waxes. The cryo-adhesive method **[53]** and the cellulose-acetate method **[54]** both isolate the top-level of the leaf waxes. Both are mechanical methods, and as such they cannot extract intracuticular waxes without extracting the insoluble polymer matrix. These methods have been claimed mainly to isolate the epicuticular waxes **[53, 54],** leaving the actual barrier (*i.e.* the intracuticular waxes) largely unaffected **[55]**. In Paper II a chloroform-methanol extraction method was used **[56]**. With this method solvent molecules are able to reach the deeper layers of the cuticle and an extract of both epi- and intracuticular waxes is obtained **[57-58]**. Cuticle wax was extracted with chloroform/methanol from the *adaxial* side of *Clivia* leaves and the chemical composition of the extract was de-

termined by GC-MS. The extract contained 68% primary alcohols (C_{16}-C_{32}, centred at C_{28}) and 16% n-alkanes (C_{21}-C_{33}, centred at C_{31}), full details on the extract composition are given in Paper II. 96% of the alcohols are comprised by $C_{26}H_{53}OH$ - $C_{32}H_{65}OH$, but the extract also contains shorter alcohols. 92% of the n-alkanes are comprised by $C_{25}H_{52}$ – $C_{33}H_{68}$, and hydrocarbon chains with an odd number of carbon atoms dominate, but the extract also contain n-alkanes that are shorter or have an even number of carbon atoms. Compared to leaf waxes from common crop plants like wheat (*Triticum aestivum*) **[60]** and barley (*Hordeum vulgare L.)* **[61],** a common feature is the high content of primary alcohols (72 and 87%, respectively) and the relatively low content of n-alkanes (5 and 1%, respectively). The alcohols in wheat are dominated by $C_{28}H_{57}OH$ (66%) and in barley by $C_{26}H_{53}OH$ (80%). The chain-lengths of the main n-alkane components are C_{27}-C_{33} in wheat and C_{31}-C_{33} in barley. Enzymatically isolated cuticle, $CHCl_3$/MeOH extracted *Clivia* wax, and extracted wax in excess water (50 wt%) were compared using DSC to map the thermotropic phase behaviours (Fig. 7).

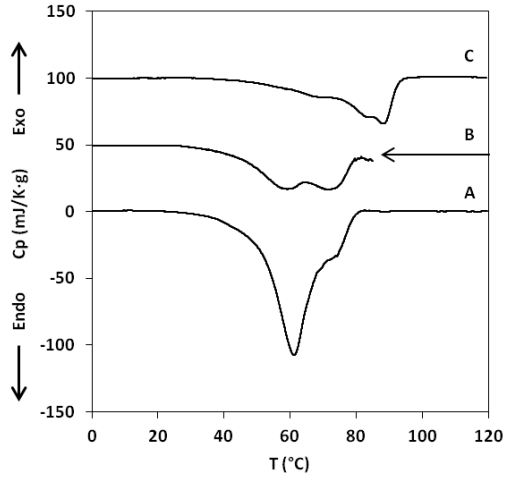

Figure 7. *Thermograms of:* ***(A)*** *extracted Clivia wax,* ***(B)*** *extracted Clivia wax with 50 wt% water, and* ***(C)*** *enzymatically isolated cuticle. Offset +50 mJ/K·g per curve, scan rate 1 °C/min.*

Extracted *Clivia* wax shows a broad pronounced transition peak ($T_{1,\ max}$=61 °C) followed by a smaller shoulder ($T_{2,\ max}$=74 °C). The total transition covers a temperature range from 30 to 80 °C, with a transition enthalpy of 137 J/g. When the wax is immersed in excess water (50 wt%) the two transition temperatures are more or less preserved ($T_{1,\ max}$=59 °C and $T_{2,\ max}$=72 °C) while the

transition enthalpy of the first peak is significantly decreased. The total transition enthalpy for hydrated wax is 44 J/g wax. The enzymatically isolated cuticle membrane shows a broad transition region that starts at 30 °C and ends at 95 °C (ΔH=44 J/g). Two peaks appear at $T_{1, max}$=83 °C and $T_{2, max}$=88 °C, probably originating from the polymer network **[62]**. The transitions attributed to the extractable wax are barely visible, which reflects the fact that the cuticle only comprises about 20 wt% wax **[63]**.

Surfactant structural effects on isolated cuticle

The diffraction patterns of ground cuticles were evaluated at 25 °C. SAXD of cuticles equilibrated at 50 and 85% RH are compared to dry cuticle and dry re-crystallized extracted wax, figure 8A. Re-crystallized extracted cuticle wax displays a lamellar phase with a repeat distance of q= 1.64 nm^{-1} (d= 3.83 nm). The untreated cuticle shows a small indication of a peak in the curve at approximately the same spacing, at both dry and humid conditions. This indicates that the diffraction peak in the cuticle originates from wax entities within the cuticle, and that the same structure is retained after re-crystallization of the wax. The cuticle is a complex matrix **[8]** and long-range order is present in cuticles from most plants **[14]**. However, some plants (like *E. myrsinites*, *S. striatum*, *Lactuca sativa* and *Juniperus communis*) lack long range order in their cuticle wax **[14]**. The short range order in the cuticle was evaluated by WAXD. The WAX diffraction traces of dry cuticle as a function of temperature are shown in figure 8B. The *Clivia* cuticle shows orthorhombic hydrocarbon chain packing with a main peak at approximately q=15.1 nm^{-1} (d=0.416 nm) and a smaller peak at q=16.6 nm^{-1} (d=0.378 nm). The main peak shifts slightly to lower q, and the small peak disappears above 65 °C, indicating a transition from orthorhombic to hexagonal hydrocarbon chain packing. As the temperature increases, parts of the wax turn amorphous and give rise to a shoulder just below q=14 nm^{-1}. The cuticle equilibrated at 50 RH% (Fig. 8C) maintains a trace of the orthorhombic peak even at higher temperatures. At this relative humidity other smaller peaks are apparent at approximately: q=9.54, 10.9, and 11.5 nm^{-1} (d=0.659, 0.576, and 0.546 nm). The peak at q=11.5 nm^{-1} tentatively may come from triterpenoids **[64]**. The small peaks do not move as a function of temperature or humidity, but loose intensity when surfactant is present (see below). The cuticle equilibrated at 85 RH% (figure 8D) shows similar behaviour. The peak attributed to an orthorhombic structure at 0.378 nm does not re-emerge when temperature is lowered, probably due to insufficient time for the molecular rearrangement, but traces of the smaller peaks at higher d-spacings reappear.

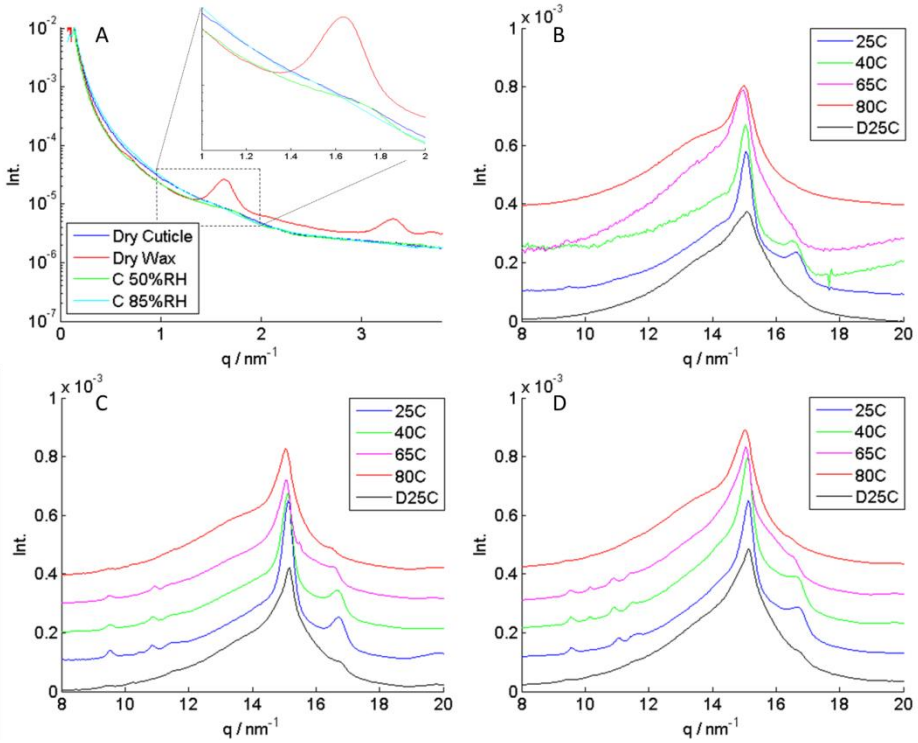

Figure 8. *SWAXD of intact cuticle without surfactant present. A: SAX diffraction traces at 0, 50, and 85 RH%, where: C=Cuticle, compared to recrystallized cuticle wax. WAX diffraction traces of cuticle as a function of temperature. B: dry cuticle, C: cuticle equilibrated at 50 RH%, D: cuticle equilibrated at 85 RH%.*

Model cuticle wax

The structure and ordering of the cuticle has been investigated and described in detail. Furthermore, some insight has been gained in how humidity affects the cuticle characteristics. With this at hand, efforts were made to design a model of the limiting barrier in the cuticle, *i.e.* the plant leaf intracuticular wax (IW), with the aim to be used to estimate effects of formulations on cuticle diffusivity *in vitro* (Paper II). The thermotropic (25-80 °C) and lyotropic (water) phase behaviour and the structure of individual phases in the model wax – water system was determined. The model was developed based on data obtained through analysis and characterization of cuticle wax from *Clivia* leaves (Fig. 7, Paper II).

Model wax composition

1-docosanol ($C_{22}H_{45}OH$) and dotriacontane ($C_{32}H_{66}$) were chosen as constituents of the tentative model cuticle wax based on their resemblance to the two most abundant aliphatic chemical compound classes in *Clivia* leaf and other commercially important plant leaf waxes (*c. f.* Paper II). The simplicity of the model wax system facilitates the observation of physical-chemical interactions that would be enveloped and difficult to interpret in a native or more complex model system. The phase behaviour of dry 1-docosanol and 1-tetracosanol was reported by Precht and co-workers in 1976 **[65]**, but to the best of our knowledge, the longest primary alcohols to be investigated in a binary phase diagram with water are hexadecanol(C_{16}) and octadecanol(C_{18}) **[66]** where the ability of the alcohols to form hemihydrates is discussed. The highest alkane/alcohol mixture described is that of hexadecane(C_{16})/hexadecanol(C_{16}) **[67],** revealing the space groups and unit cell parameters. The miscibility of n-alkanes and alcohols in the solid state is very low even if their chain lengths are matched and rather short (c.f. hexadecane/hexadecanol **[67]**), and they do not co-crystallize. Therefore, the choice of an alcohol with a slightly shorter chain length than the median in the cuticle wax extract, together with a longer alkane, was adopted to mimic the distribution of hydrocarbon chains in the native wax. The phase triangle (Fig. 9) served as map when the thermotropic phase behaviour of the system was characterized by DSC and PLOM along four sections of the triangle: **A** ($C_{22}H_{45}OH$ / $C_{32}H_{66}$), **B** ($C_{32}H_{66}$/H_20), **C** ($C_{22}H_{45}OH$ /H_20) and **D** ({$C_{22}H_{45}OH$ / $C_{32}H_{66}$}/H_20, 50/50). Micrographs illustrating the phase transitions in the dry model wax system are presented in figure 10. Transition temperatures, enthalpies and entropies for phase transitions detected in the system are summarized in table 1. SWAXD was used to determine the structure of the individual phases (Table 2). The entire data set was used to construct binary phase diagrams (Figures 11-14), comprising the lines A-D in figure 9.

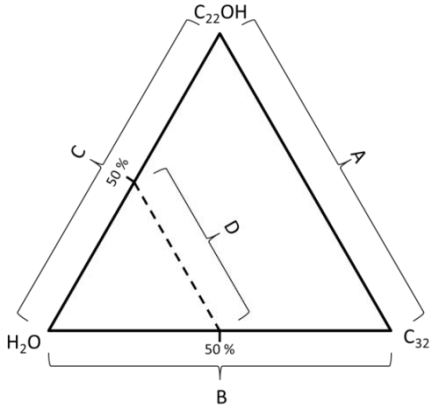

Figure 9. *Phase triangle of the $C_{22}H_{45}OH/C_{32}H_{66}/H_20$ system.* ***A*** *($C_{22}H_{45}OH$ / $C_{32}H_{66}$),* ***B*** *($C_{32}H_{66}/H_20$),* ***C*** *($C_{22}H_{45}OH$ /H_20) and* ***D*** *({$C_{22}H_{45}OH$ / $C_{32}H_{66}$}/H_20, 50/50).*

Table 1. *The temperature, enthalpy and entropy of phase transitions observed in the $C_{22}H_{45}OH/C_{32}H_{66}/H_20$ system. Changes in enthalpy and entropy are calculated per mol (or mass) of compound below the transition, except the melting of the hemihydrate which is per mol (or mass) of $C_{22}H_{45}OH{\cdot}½H_2O$.*

Phase transition			T (°C)	ΔH (kJ/mol)	ΔH (J/g)	ΔS (J/mol K)
Dry						
$C_{22}OH(M)$	→	I.L.	71.6	82.0	251	238
$C_{32}(O)$	→	$C_{32}(T_{RIII})$	64.2	32.2	71.4	95.6
$C_{32}(T_{RIII})$	→	I.L.	69.2	74.2	165	217
$C_{22}OH(M)$+ $C_{32}(T_{RIII})$	→	I.L.	64.9 (Eutectic)			
Wet						
$C_{22}OH(M)$	→	$C_{22}OH(H_c)$	60.7	28.2	86.3	84.5
$C_{22}OH(H_c)$	→	I.L.	73.4	52.6	157	152
$C_{32}(O)$	→	$C_{32}(T_{RIII})$	64.2	32.2	71.4	95.6
$C_{32}(T_{RIII})$	→	I.L.	69.2	74.2	165	217
$C_{22}OH(H_c)$+ $C_{32}(T_{RIII})$	→	I.L.	65.6 (Eutectic)			

I.L.: isotropic liquid, C_{32} (T_{RIII}): triclinic crystalline rotator phase, C_{32} (O) and $C_{22}OH$ (M): orthorhombic alkane and monoclinic alcohol crystalline phases, respectively. $C_{22}OH$ (H_c): hexagonal crystalline hemihydrate.

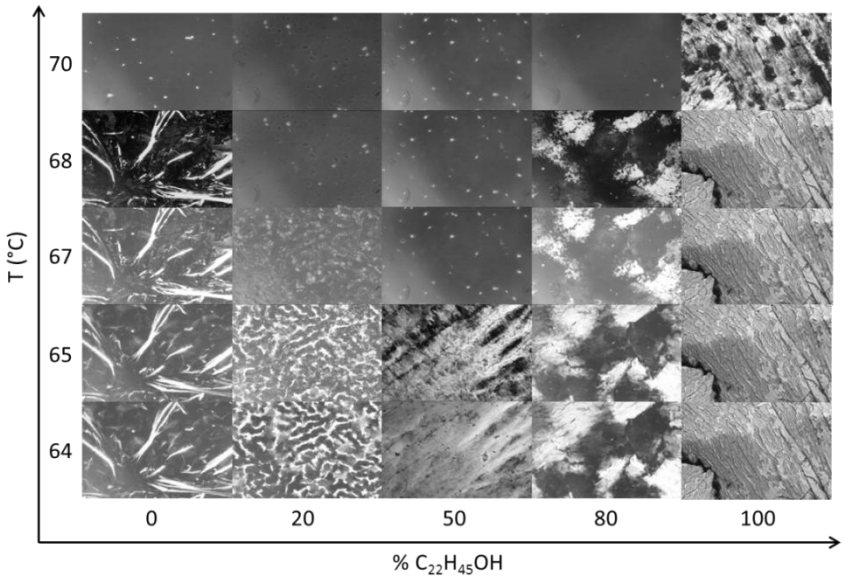

Figure 10. *PLOM micrographs of binary mixtures of $C_{22}H_{45}OH/C_{32}H_{66}$ vs. temperature (64-70 °C), (c.f. phase diagram in figure 11).*

PLOM images of binary mixtures of $C_{22}H_{45}OH$ / $C_{32}H_{66}$ vs. temperature (64-71 °C) are shown in figure 10. Dotriacontane forms needle like highly birefringent crystals over a more or less transparent background and melts at 69.2 °C. 1-docosanol appears as a continuous birefringent film and melts at 71.6 °C. Mixtures with high amounts of 1-docosanol follows a similar pattern as the pure alcohol. However, when dotriacontane is the main component a strongly birefringent network is observed, against a more transparent background. The thermotropic phase behaviour of mixtures of $C_{22}H_{45}OH$, $C_{32}H_{66}$, and H_20 is depicted in the binary phase diagrams (Figs. 11-14). Each diagram corresponds to one of the lines A, B, C and D in figure 9.

$C_{22}H_{45}OH/C_{32}H_{66}$

The phase behaviour of the dry model wax $C_{22}H_{45}OH/C_{32}H_{66}$ is presented in figure 11. Below 64.9 °C the two components are present as separate crystalline phases, but $C_{32}H_{66}$ transforms to a rotator phase at 64.2 °C. Above the eutectic transition line at 64.9 °C three different regions are visible, from the left: i) an isotropic liquid comprising the two components together with $C_{32}H_{66}$ in a crystalline state, ii) isotropic liquid and iii) crystalline $C_{22}H_{45}OH$ together with isotropic liquid. The eutectic meets the liquidus line at a temperature of 64.9 °C and a composition of 40.3 % $C_{22}H_{45}OH$. Rotator phases in pure alkanes

have previously been described by others **[48, 68]**, where dotriacontane is reported to form a T_{RIII} phase at 64.0 ±0.5 °C upon heating **[68]**. Eutectic transitions have been discussed for other related systems **[69, 70]**. In the binary phase diagram given in figure 11 pure 1-docosanol melts at 71.6 °C and pure dotriacontane melts at 69.2 °C which corresponds well with literature data (72 °C) **[71]** and (69 °C) **[72]** respectively. The enthalpy of melting is 251 J/g for pure $C_{22}H_{45}OH$ and 236 J/g for pure $C_{32}H_{66}$, where the rotator transition accounts for 71.4 J/g. This corresponds to a molar enthalpy of melting for the two components of 82.0 kJ/mol and 106 kJ/mol, respectively, which is in good agreement with literature: 82.8±6.0 kJ/mol ($C_{22}H_{45}OH$) **[70, 73]**, 118 kJ/mol ($C_{32}H_{66}$) **[72]**. The enthalpy for total sample melting is rather invariant to the mass composition of the model wax, 247±5 J/g, (*i.e.* ±2% of ΔH_{melt} of pure $C_{22}H_{45}OH$). The liquidus line in figure 11 was fitted using the Shreder equation (Eq. 9, **[74]**) in combination with the Flory-Scatchard approach on linear polymers (Paper II) to account for non-ideality of the liquid.

$$\ln a_i = \frac{\Delta H_{melt}}{R}\left(\frac{1}{T^0} - \frac{1}{T}\right) \qquad \text{(Eq. 9)}$$

Where a_i is the activity of component i (in this case $C_{22}H_{45}OH$ or $C_{32}H_{66}$), ΔH_{melt} and T^0 is the heat effect and the melting temperature of pure component i, while T is the melting temperature of the mixture. The Shreder equation describes the composition of a liquid phase x_i in equilibrium with a pure solid phase **[75]**. However, activity a_i was used, and the relation between activity and composition was established using the Flory-Scatchard approach in order to account for association of the alcohol **[76]**.

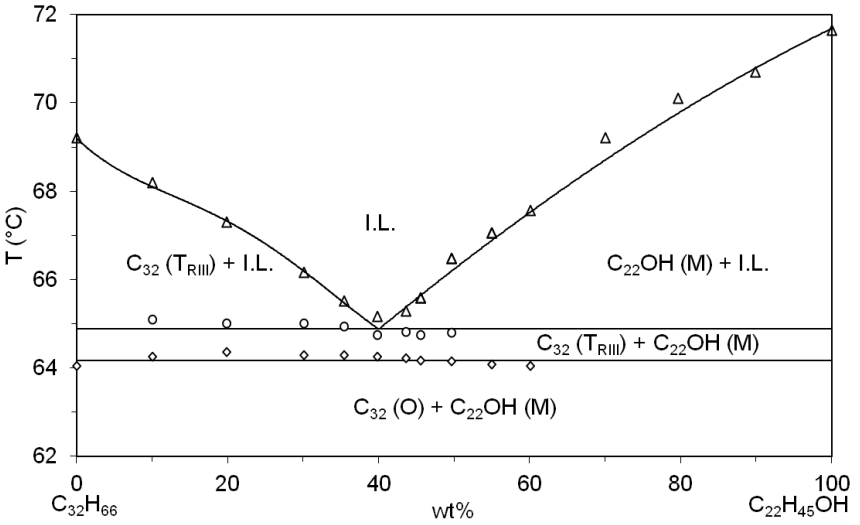

Figure 11. *Binary phase diagram of 1-docosanol/dotriacontane. I.L.: isotropic liquid, C_{32} (T_{RIII}): triclinic crystalline rotator phase, C_{32} (O) and C_{22}OH (M): orthorhombic alkane and monoclinic alcohol crystalline phases, respectively. Data points obtained by DSC; Rhombi: C_{32} (O) to C_{32} (T_{RIII}) transition, Circles: system eutectic transition, Triangles: endpoint of melting. Lines: C_{32} (O) to C_{32} (T_{RIII}) isothermal transition at 64.2 °C, eutectic isothermal transition at 64.9 °C and liquidus calculated using the Shreder equation and the Flory-Scatchard approach.*

Model wax - water phase behaviour

1-docosanol melts at 71.6 °C, which is in agreement with literature data (72 °C) **[66]**. Water induces a phase transition at lower temperature (60.7 °C) followed by a second phase transition at 73.4 °C. This indicates some interaction between the alcohol and water. The water solubility in 1-docosanol at 60.7-73.4 °C is 2.7 % (w/w). This corresponds to one water molecule per two alcohol molecules. Above 73.4 °C the solubility is below the detection limit of 0.1 % (w/w). In comparison, 1-docosanol solubility in water was determined at 68 °C to 0.0094 % (w/w), and at 80 °C the solubility is 0.025 % (w/w). The alcohol solubility in water could not be detected below its first phase transition at 60.7°C. Dotriacontane shows a phase transition at 64.2 °C and melts at 69.2 °C, which corresponds well with literature data (64 and 69 °C) **[77, 78]**. Apart from the phase transition in dry dotriacontane at 64.2 °C, another transition exists in a wide range of compositions at around 64.9 °C. This indicates the presence of an eutectic point in the system. The solubility of dotriacontane in water and *vice versa* in the temperature range 20-100 °C was

below the detection limit of the method used. This indicates that interactions between the alkane and water are absent. The ternary system 1-docosanol/dotriacontane/water has a slightly higher eutectic point at 65.6 °C. SWAXD was employed to resolve the structure of the individual phases in the pure, mixed and hydrated samples (Table 2).

Table 2. *Bragg peaks (d) of model wax constituents in dry and hydrated (50 wt% water) state. Weak peaks are given in parenthesis (c.f. Figure 11-15).*

	$C_{22}H_{45}OH$, dry						$C_{22}H_{45}OH$, excess water					
T (°C)	d (Å)					Unit cell	d (Å)					Unit cell
25	50.2	*(4.28)*	4.10	*(3.95)*	3.64	M	50.2	*(4.28)*	4.10	*(3.96)*	3.65	M
54	-	-	-	-	-	-	50.2	*(4.30)*	4.12	*(4.00)*	3.69	M
55	50.5	*(4.30)*	4.12	*(4.00)*	3.69	M	-	-	-	-	-	-
58	-	-	-	-	-	-	50.5	*(4.30)*	4.13	*(4.01)*	3.70	M
60	50.5	*(4.30)*	4.13	*(4.01)*	3.70	M	62.6	-	4.18	-	-	
62	-	-	-	-	-	-	62.6	-	4.19	-	-	H_c
64	-	-	-	-	-	-	62.1	-	4.19	-	-	H_c
65	50.5	*(4.30)*	4.13	*(4.02)*	3.71	M	-	-	-	-	-	-
70	-	-	-	-	-	-	62.1	-	4.22	-	-	H_c
72	-	-	-	-	-	-	*(63.1)*	-	-	-	-	-
74	-	-	-	-	-	-	-	-	-	-	-	-
	$C_{32}H_{66}$, dry						$C_{32}H_{66}$, excess water					
T (°C)	d (Å)					Unit cell	d (Å)					Unit cell
25	42.8	4.14	3.76	(3.70)		O	42.8	4.14	3.75	(3.69)		O
58	42.8	4.17	3.81	(3.76)		O	42.8	4.16	3.80	(3.75)		O
60	42.6	4.16	3.83	(3.76)		O	42.6	4.16	3.82	(3.75)		O
66	41.3	4.25	4.12	4.07		T_{RIII}	41.5	4.23	4.15	4.09		T_{RIII}
70	-	-	-	-	-	-	-	-	-	-	-	-

M: Monoclinic, H_c: Hexagonal, O: Orthorhombic, T_{RIII}: Triclinic rotator III

$C_{22}H_{45}OH/H_2O$

The binary phase diagram in figure 12 shows the phase behaviour of the system $C_{22}H_{45}OH/H_2O$. Below 60.7 °C the system comprises a monoclinic crystalline phase of $C_{22}H_{45}OH$ in equilibrium with water. Above this temperature a hexagonal crystalline phase is formed in the presence of water ($C_{22}H_{45}OH \cdot ½H_2O$), which melts at 73.4 °C. This hemihydrate prevails in excess water, while at low water content (less than 2.7%) it co-exists with the monoclinic crystal up to 71.6 °C, as well as an isotropic liquid phase of $C_{22}H_{45}OH$ (71.6-73.4 °C). Above 73.4 °C two phases are present at all compositions, the isotropic liquid and water.

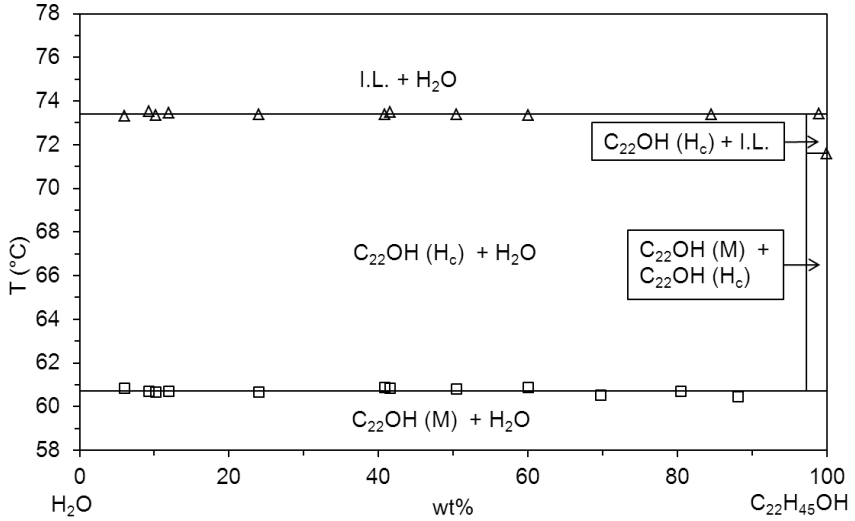

Figure 12. *Binary phase diagram of 1-docosanol/water. I.L.: isotropic liquid, $C_{22}OH$ (H_c): hexagonal crystalline phase ($C_{22}H_{45}OH \cdot ½H_2O$), $C_{22}OH$ (M): monoclinic crystalline phase. Data points obtained by DSC; Squares: $C_{22}OH$ (M) to $C_{22}OH(H_c)$ transition, Triangles: onset of melting. Lines: $C_{22}OH(M)$ to $C_{22}OH(H_c)$ isothermal transition at 60.7 °C, liquidus isothermal transition at 73.4 °C, hydrate-line isocompositional (60.7 - 73.4 °C) at 97.3% $C_{22}H_{45}OH$.*

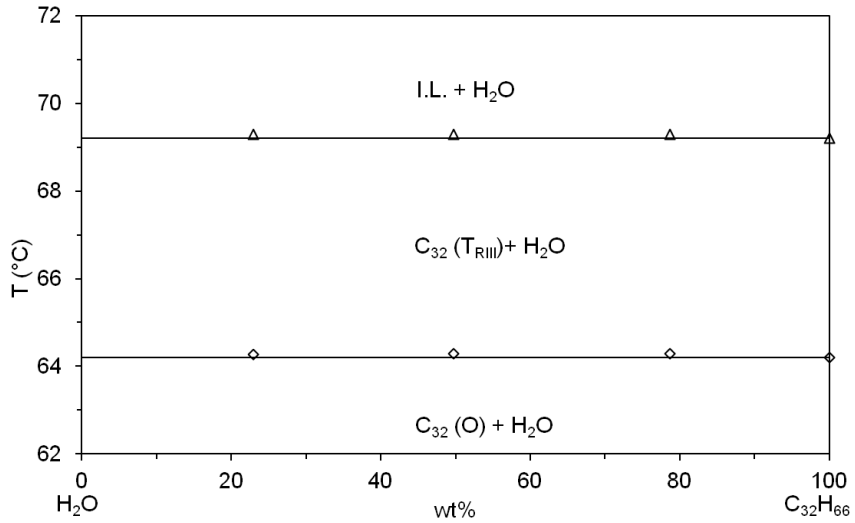

Figure 13. *Binary phase diagram of dotriacontane/water. I.L.: isotropic liquid, C_{32} (T_{RIII}): triclinic crystalline rotator phase, C_{32} (O): orthorhombic crystalline phase. Data points obtained by DSC; Rhombi: C_{32} (O) to C_{32} (T_{RIII}) transition, Triangles: onset of melting. Lines: C_{32} (O) to C_{32} (T_{RIII}) isothermal transition at 64.2 °C, liquidus isothermal at 69.2 °C.*

$C_{32}H_{66}/H_2O$

The binary phase diagram in figure 13 shows the phase behaviour of the system $C_{32}H_{66}/H_2O$. Below 64.2 °C the system comprises an orthorhombic crystalline phase of $C_{32}H_{66}$ in equilibrium with water. At 64.2 °C a triclinic rotator phase (T_{RIII}) is formed instead, and above 69.2 °C two phases are present at all compositions: liquid $C_{32}H_{66}$ and water.

$C_{22}H_{45}OH/C_{32}H_{66}/H_20$

The phase behaviour of the hydrated model wax $C_{22}H_{45}OH/C_{32}H_{66}/H_20$ is presented in figure 14. Below 60.7 °C the alcohol and the alkane are present as separate crystalline phases in equilibrium with water. The $C_{22}H_{45}OH\cdot$ ½H_2O hemihydrate forms at 60.7 °C, and the $C_{32}H_{66}$ rotator phase forms at 64.2 °C. Above the eutectic transition line at 65.6 °C three different regions are visible, from the left: i) $C_{32}H_{66}$ triclinic rotator phase (T_{RIII}), isotropic liquid and water, ii) isotropic liquid and water and, iii) $C_{22}H_{45}OH\cdot$ ½H_2O hexagonal hemihydrate, isotropic liquid and water. The eutectic meets the liquidus line at a temperature of 65.6 °C and a $C_{22}H_{45}OH$ content of 33.8%. At the eutectic point four phases are present at the same time (*c. f.* Gibbs Phase Rule **[17]**).

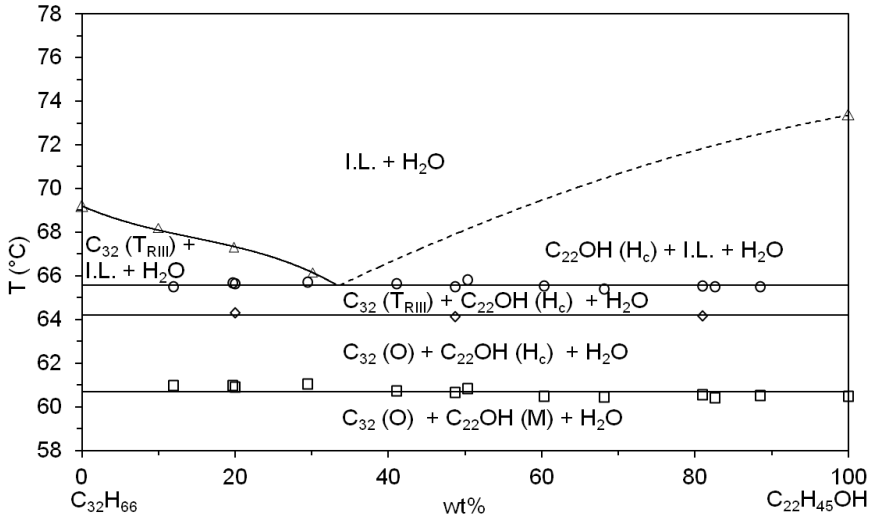

Figure 14. *Ternary phase diagram of 1-docosanol/dotriacontane/water (i.e. ($C_{22}H_{45}OH/C_{32}H_{66}$)/ H_2O, 50/50 by weight). I.L.: isotropic liquid, C_{32} (T_{RIII}): triclinic crystalline rotator phase, $C_{22}OH$ (H_c): hexagonal crystalline phase ($C_{22}H_{45}OH \cdot$ ½H_2O), C_{32} (O) and $C_{22}OH$ (M): orthorhombic alkane and monoclinic alcohol crystalline phases, respectively. Data points obtained by DSC; Squares: $C_{22}OH$ (M) to $C_{22}OH$ (H_c) transition, Rhombi: C_{32} (O) to C_{32} (T_{RIII}) transition, Circles: system eutectic transition, Triangles: endpoint of melting.*

Lines: $C_{22}OH$ (M) to $C_{22}OH$ (H_c) isothermal transition at 60.7 °C, C_{32} (O) to C_{32} (T_{RIII}) isothermal transition at 64.2 °C, eutectic isothermal transition at 65.6 °C, and liquidus calculated using the Shreder equation and the Flory-Scatchard approach.

This phase diagram was constructed partly by using data from the dry system (the liquidus line on the alcohol side of the eutectic, dotted line in figure 14). Dotriacontane does not interact with water. Hence, the liquidus fitting of the alkane branch using the Flory-Scatchard approach from the dry system could also be used for the wet case. The alcohol, however, forms a hydrate which melts at 1.8 °C higher than the monoclinic crystalline form. To construct the alcohol branch of the liquidus in figure 14, the same parameters as for the dry system were used, except for the enthalpy of melting of the alcohol that was taken as the sum of the two transitions of the wet alcohol. The data given in figures 11-14 were compiled to illustrate the ternary phase behaviour of the system with respect to temperature (Figure 15). Although schematic in their nature and not to scale (to facilitate visibility) the diagrams acknowledge thermodynamic laws at all points within the triangles.

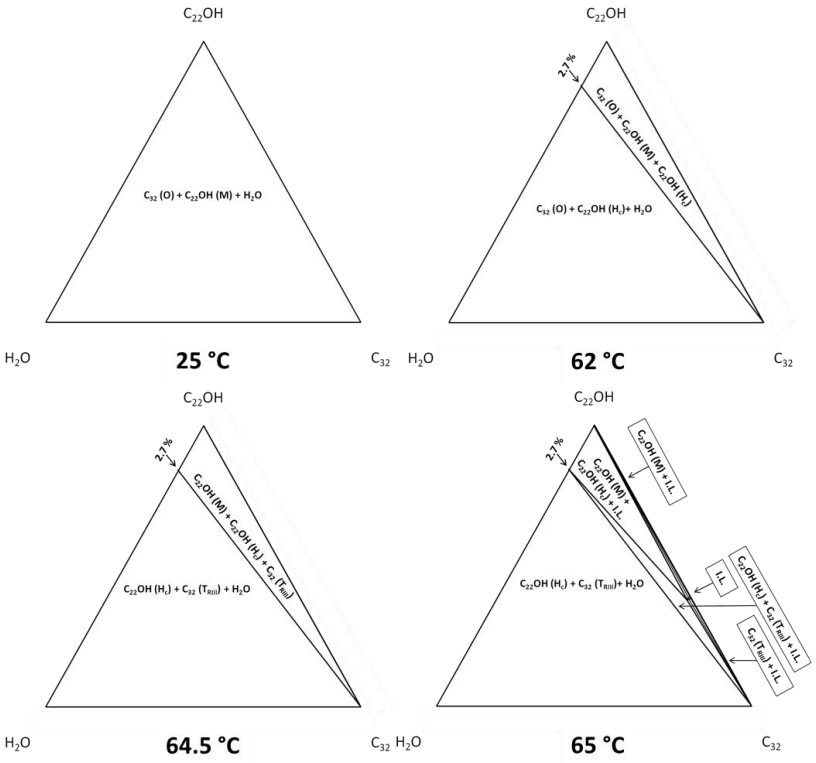

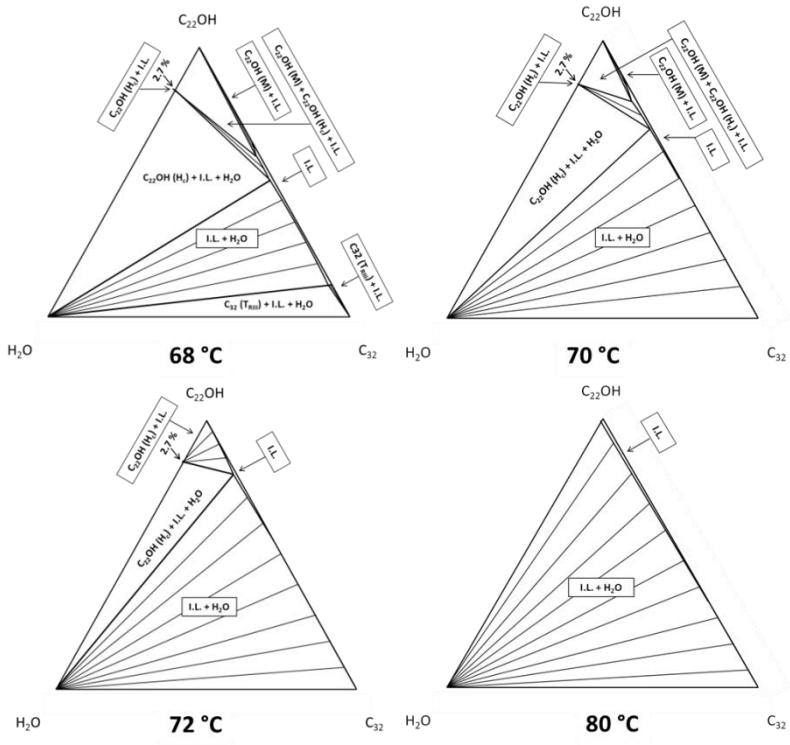

Figure 15. *Schematic ternary phase diagrams of 1-docosanol/ dotriacontane/ water at fixed temperatures. I.L.: isotropic liquid, C32 (TRIII): triclinic crystalline rotator phase, C22OH (Hc): hexagonal crystalline phase (C22H45OH · ½H2O), C32 (O) and C22OH (M): orthorhombic alkane and monoclinic alcohol crystalline phases, respectively.*

Model wax validation

Cuticle wax contains many different compounds with characteristic properties. Furthermore, compounds interact and create a complex system, probably partly amorphous in nature. Individual phase transitions may very well be hidden in the broad transition peaks of figure 7. Dry extracted *Clivia* wax displays a broad pronounced transition peak at 61 °C, followed by a smaller shoulder at 74 °C. In presence of water, the positions of these peaks are more or less preserved (59 and 72 °C, respectively) while the transition enthalpy of the first peak is significantly decreased. The total transition enthalpy of the hydrated wax corresponds to one third of that for the dry wax, which reflects a large effect of water. The enzymatically isolated cuticle membrane shows two pronounced peaks at 83 and 88 °C, which may be attributed to transi-

tions in the cutin-cutan polymer network. Here the wax phase transitions are hidden in the long preceding slope, starting at 30 °C. The transitions in the model waxes clearly fall in the transition window of the extracted leaf waxes. The transition enthalpy for dry extracted *Clivia* wax was 137.1 J/g. Other extracted plant waxes have melting enthalpies in the range of 130 - 200 J/g **[61, 79, 80]**. The total transition enthalpy is lower for the cuticle waxes than for the model wax mixtures (248 J/g), which implies that the complex cuticle wax is more disordered and contains a larger fraction of amorphous material.
The features shown by the micrographs in figure 10 correspond to coexistence of a $C_{32}H_{66}$ triclinic rotator phase (T_{RIII}) and a $C_{22}H_{45}OH$ monoclinic alcohol phase (M), and their melting (*c.f.* phase diagram in Figure 11). The presence of different domains in the wax matrix relates to what have been shown for other reconstituted native plant waxes **[19, 20, 61, 79, 81]** and model systems thereof **[82]**. As a further remark it should be acknowledged that there might be other phase transitions than those of the wax itself occurring below 80 °C. Sachleben and co-workers used NMR to study the polymer network of the cuticle **[62]**. They reported that cutan is crystalline below 87 °C, while cutin on the other hand, has a glass transition below 60 °C and is in a rubbery state above this temperature. Cutin could potentially induce wax monomer melting, or allow for a larger part of the wax molecules to stay in an amorphous phase even at lower temperatures. The volume of disordered wax monomers surrounding the cutin polymer network strands could thus be a major diffusional pathway for hydrophobic solute molecules **[8]**.

Surfactant solutions

The characteristics of the cuticle in terms of its content and thermotropic phase behaviour are crucial to evaluate in order to understand the process of AI cuticle penetration. But the information is not complete until the structure and ordering of the individual building-blocks that comprise the barrier can be explained, and how surfactant absorption affecting this structure is known. Therefore, X-ray diffraction was used to determine the aggregate structure of surfactant/water solutions, and how absorption of surfactant affects the cuticle.

Surfactant water sorption

In this thesis two surfactants ($C_{10}EO_7$ and $C_8G_{1.6}$) were used together with one AI (tebuconazole) as a model compound. The chemical structures of these compounds are shown in figure 16.

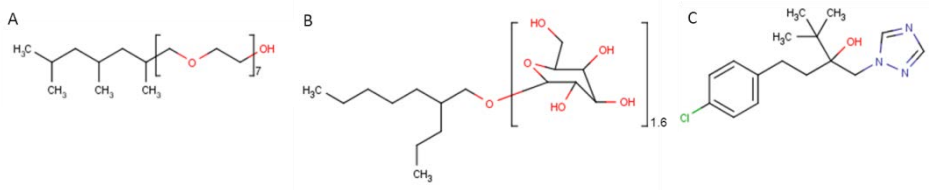

Figure 16. *Chemical structure of surfactants and active ingredient. A: $C_{10}EO_7$, B: $C_8G_{1.6}$, C: tebuconazole.*

$C_{10}EO_7$ with a straight hydrocarbon chain (hepta (ethylene glycol) mono n-decyl ether) should go through two phase transitions as the water content increases at 25 °C (liquid to hexagonal at around 30 wt% water, and hexagonal to liquid at around 57 wt% water, **[83]**). This may however not be true for the technical grade of $C_{10}EO_7$ with a branched chain, which is commonly used in agricultural spray applications, and investigated in this study (Fig. 16A). Sorption calorimetry and water activity measurements were used to investigate phase transitions upon hydration of the surfactant, and the relation between water content in a sample and its corresponding water activity, both at 25 °C. The range in sample hydration resembles conditions on the leaf surface as water evaporates from the formulation. Figure 17A shows the $C_{10}EO_7$ water sorption isotherm at 25 °C and figure 17B the partial molar enthalpy of mixing for water.

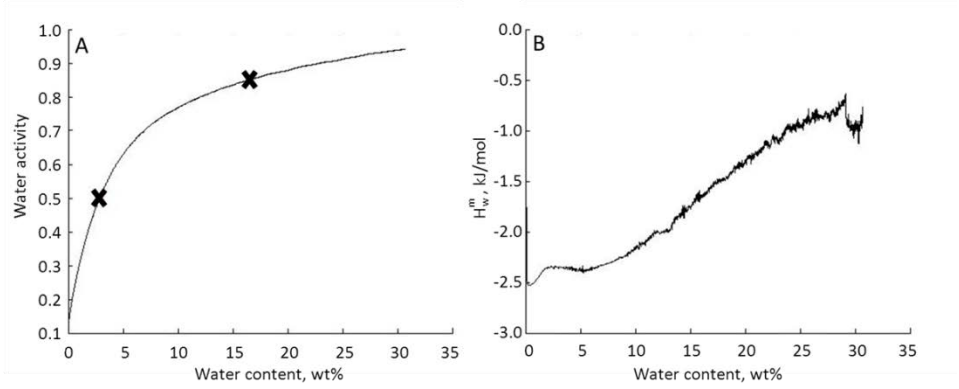

Figure 17. *A: $C_{10}EO_7$ water sorption isotherm, solid line obtained using sorption calorimetry, x obtained with Novasina, B: partial molar enthalpy of mixing of water in the $C_{10}EO_7$ – water system, obtained using sorption calorimetry. Both curves at 25 °C.*

Table 3 shows the water activity and the clouding temperature of the surfactant solutions used in this study. It is clear from the sorption isotherm in figure 17A that no major events take place as the water activity increases from close to zero to 0.94. At the highest water activity, the mass fraction of water in the sample is close to 30 wt%. Thus, viewing the data in figure 17 it is possible that a transition would occur at higher water content. This was checked with polarized light microscopy (Tab. 3) and no transition except clouding could be observed in the 10 to 95 wt% water content range and temperature range of 25 to 100 °C. Hence, this surfactant does not undergo any major phase transitions during the application procedure. Prior to application the surfactants are diluted from concentrated solutions and mixed with water in a spray tank. Complete dissolution can be facilitated by the fact that the concentrate does not undergo any phase transition upon dilution.

Table 3. *Characteristics of surfactant solutions.*

Surfactant solution (wt % $C_{10}EO_7$)	a_w	Clouding T. (°C)
1	1	55.5
4	1	56.5
25	0.997	62.6
50	0.988	79.4
83.5	0.85	>100
97.2	0.50	>100

Surfactant solutions

Potential changes of surfactant aggregate structure in solutions as a function of concentration was investigated by SWAXD and the results are shown in figure 18. The solution undergoes changes as water activities decrease and surfactant concentrations increase. In SAXD (Fig. 18A) a small peak is observed at q=1.48 nm^{-1}, which indicates spherical micelles in the solutions that contain 1 to 20 % surfactant **[17]**. In the 25% solution, the micelles have grown to ellipsoidal shapes **[85]**, resembling a more rod-like structure **[86]**. The peak originally at q=1.48 nm^{-1} has moved to q=1.82 nm^{-1}. A peak is also present just above q=1.13 nm^{-1}, which arises from the structure-factor of the micelles in solution **[87]**. In WAXD (Fig. 18B) a peak corresponding to bulk water is observed at q=20nm^{-1} for the solutions that contain 1 to 25 % surfactant **[84]**. With 50% surfactant a signal from the liquid hydrocarbon chains is clearly visible at around q=14 nm^{-1} (d=0.42 nm) **[88-90]**. This bump increases in size to form a distinct peak at higher surfactant concentrations, as more hydrocarbon chains are present in the sample.

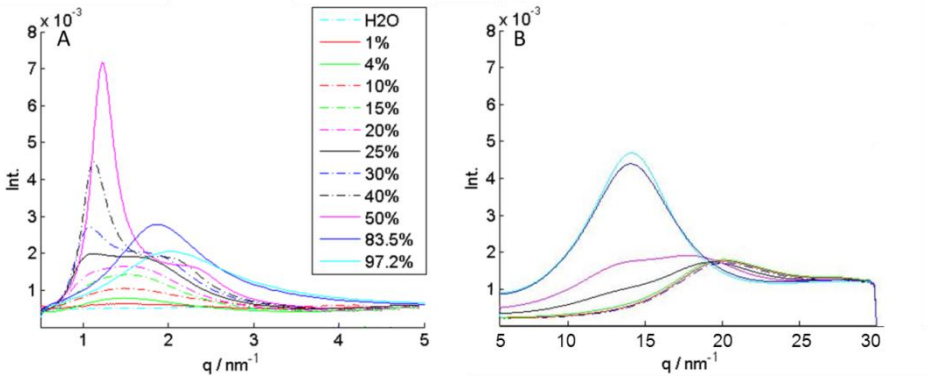

Figure 18. *Diffraction curves of water and surfactant solutions (aq.) at 25 °C, 83.5% and 97.2% corresponds to 85RH% and 50RH% respectively, A: SAXS, B:WAXS.*

In solutions that contain 30 to 50 % surfactant, elongation and growth of the micellar aggregates occur. At higher surfactant concentrations (83.5 and 97.2%) the system has undergone a transformation to a reverse micellar solution, with different size and scattering of the aggregates **[91, 92]**. Thus, the scattering shifts so that the structure-factor disappears while the original peak moves to around q=2.0 nm^{-1}.

Formulations design and dynamics

Surfactants can increase the solubility of hydrophobic substances in aqueous solution **[17]**. The solubility of tebuconazole as a function of surfactant concentration is shown in figure 19. This was investigated in order to establish a relationship between the tebuconazole concentration and activity in aqueous surfactant solutions. The surfactants greatly increase the solubility of tebuconazole in aqueous media (Fig. 19). To verify that all formulations provide the same steady state solute flux at a given thermodynamic activity (Eq. 1), silicone membranes were used. These are considered to be inert to surfactant induced effects. $C_{10}EO_7$, $C_8G_{1.6}$, and water formulations having the same saturation concentration of tebuconazole (80% of the solubility limit, Fig 19) produced the same initial gradient in thermodynamic activity of solute over the membrane. Consequently, very similar steady-state fluxes were obtained for silicone membranes (Fig. 20).

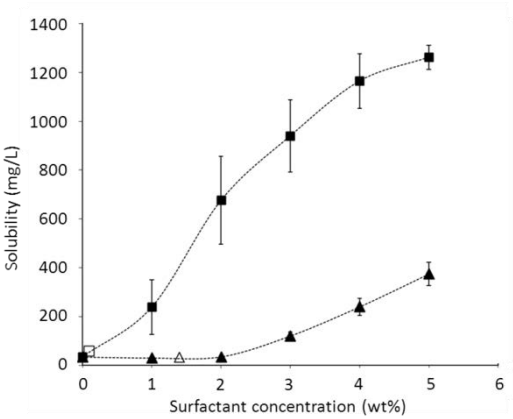

Figure 19. *Tebuconazole solubility as a function of surfactant concentration. $C_{10}EO_7$ (squares), $C_8G_{1.6}$ (triangles), solubility data (filled symbols), cmc (hollow symbols).*

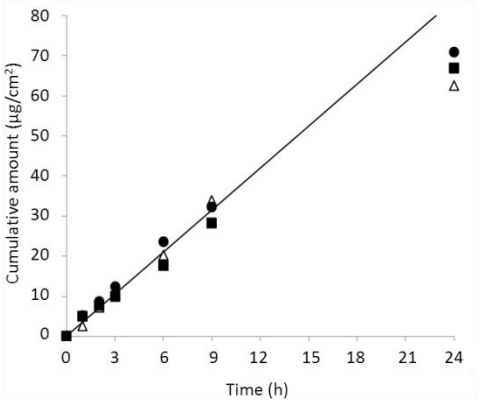

Figure 20. *Steady-state flux for $C_{10}EO_7$ (Squares), $C_8G_{1.6}$ (Circles), and water (Triangles) formulations of 0.8 tebuconazole saturation concentration over silicone membranes.*

For silicone membranes and low tebuconazole concentration (26 mg/L), pure water appears to be the most effective carrier, producing the highest release rate, followed by $C_8G_{1.6}$ and $C_{10}E_{O7}$. However, lowering the thermodynamic activity of tebuconazole decreases the driving force, which correlates well with what has previously been implicitly stated for plant CM in the literature **[8, 23]**. The subsequent decrease in flux seen with 26 mg/L tebuconazole in pure water on silicone membranes (Paper IV) is explained by the fact that the gradient in tebuconazole thermodynamic activity in the membrane is decreasing

faster when the solute concentration is low due to limited solubility in the carrier. Replacing the donor solution with fresh carrier formulation after 3, 6 and 9 hours quenched this depletion effect and thus resulted in overlapping release graphs (Paper IV) for water and the two 4 % surfactant solutions, producing close to identical steady state flux values. Hence, the data shows that the solute flux over silicone membranes is mainly governed by the gradient in thermodynamic activity, and thus not by the gradient in concentration, or by a surfactant induced increase in membrane diffusivity. Clivia leaf CM interacts with surfactants, unlike silicone, and therefore the flux cannot be described solely in terms of thermodynamic activity, c.f. **[23]**. Tebuconazole solubility in pure water is rather low, but in formulations containing surfactants the solute amounts can be significantly increased by solubilisation in micelles. Tebuconazole is not depleted from the water phase during the steady-state flux regime in the presence of surfactants since the rate of tebuconazole transfer from the micelles to the surrounding water is much faster than the flux of tebuconazole over the CM. The diffusion coefficient for tebuconazole from the micelle to the water phase is higher ($D=10^{-6}$ m^2/s, calculated using the information in **[93]** for a similar system: water-decane-$C_{12}EO_6$ and/or $C_{12}EO_8$ 2.5 wt %), than over the CM ($D=10^{-16}$ m^2/s, Paper IV). The difference is ten orders of magnitude and tebuconazole in the micelles thereby acts as a reservoir, constantly replenishing the water phase. It is also possible that surfactant molecules may accumulate at the membrane surface and thereby increase the local tebuconazole concentration. However, the exchange of tebuconazole between the surface layer and the bulk liquid is rapid. Hence, the thermodynamic activity of tebuconazole in the bulk liquid will determine the activity gradient in the membrane (da_i/dz), which in turn is the driving force for diffusion. As tebuconazole diffuses through the CM so do the surfactants. Diffusion coefficients in CM for surfactants like the ones used in this study, and tebuconazole can be similar, but their wax/water partition coefficients differ (c.f. $\log K_{cuticle/water}$(Teb.) = 3.0 (Paper IV), $\log K_{wax/water}(C_{10}EO_5) = 1.5$ **[94]**, $\log K_{wax/water}(C_{10}EO_8) = 0.75$ **[94]**). Hence, even if they have similar diffusion coefficients (D_i), the surfactant concentration in the membrane (c_i), and the flux (J_i) over the CM is lower than that for the fungicide. Since only a minor decrease of the surfactant concentration will take place during the experiments, it stays well above the CMC and saturation of the donor solution with tebuconazole will not occur.

Effects of surfactants on the cuticle

Surfactant structural effects on isolated cuticle

The diffraction patterns of ground cuticles treated with defined amounts of surfactant solution (1:1, wax:surfactant weigh ratio) were evaluated at 25 °C. SAXD of treated cuticles equilibrated at 50 and 85 RH% are compared to ground untreated cuticles equilibrated at the same RH%'s in figure 21A.

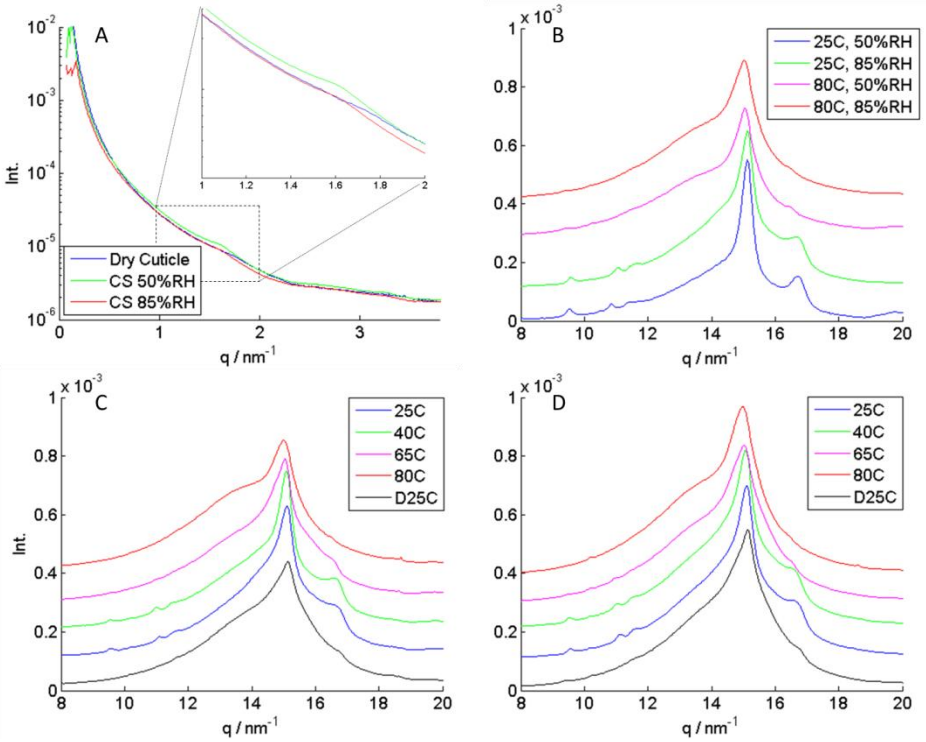

Figure 21. *SWAXD of cuticle with or without surfactant present (1:1 ratio in dry conditions). A: SAX diffraction spectra at 0, 50, and 85 RH%, where: C=Cuticle, CS=Cuticle + Surfactant. WAX diffraction spectra of cuticle as a function of temperature. B: dry untreated cuticle, C: treated cuticle equilibrated at 50 RH%, D: treated cuticle equilibrated at 85 RH%.*

The presence of 50 wt% surfactant in the cuticle sample affects the shift in transitions to lower temperatures (*c.f.* section on cuticle above and Paper I). With surfactant present the orthorhombic structures almost completely disappear at 65 °C, at both 50 and 85 RH%, while a temperature elevation to 80 °C is needed for this transition with no surfactant in the samples. In a similar manner more amorphous material appears at 65 °C for samples with surfac-

tant while 80 °C is necessary in untreated cuticle samples. Isolated cuticle has a wide transition window and transitions appear gradually in the temperature range 30-95 °C (Fig. 7). Extracted leaf waxes exhibit transitions in the range of approximately 40-80 °C in both dry and wet conditions (Fig. 7).

Surfactant induced changes in cuticle model wax I: Phase behaviour

The model of leaf cuticle wax was characterized by its phase behaviour and verified against native *Clivia* cuticle wax. The establishment of the binary (X-T) and ternary phase diagrams on model wax above offered some explanations to what actually may happen in the cuticle as it is subjected to water and surfactant. However, absorption of surfactants may change the phase behaviour of the wax.

Thermotropic phase transitions

The effect that addition of $C_{10}EO_7$, $C_8G_{1.6}$, or tebuconazole, have on thermotropic phase transitions in the model wax at different compositions ($C_{22}H_{45}OH/C_{32}H_{66}$: 100/0, 80/20, 50/50, 20/80, and 0/100) was studied by DSC. 2, 5, or 10 % of the respective substance was added to the model wax mixtures. The data are presented in figure 22. With 10% of surfactant the change in endpoint of melting was generally small, typically less than 1.6 °C ($C_{10}EO_7$) and 1.8 °C ($C_8G_{1.6}$). The eutectic transition line was lowered by maximum of 2.7 °C ($C_{10}EO_7$) and 2.1 °C ($C_8G_{1.6}$) compared to the binary model wax system. The effect of tebuconazole *vs* the two surfactants is generally stronger. The melting endpoint with 10% tebuconazole is lowered by 2.1 °C and the system starts to melt at a temperature 4.7 °C lower than the pure model wax. This is the largest effect seen in the whole data set. The RIII transition of the alkane is largely unaffected by any of the three substances used, but this transition disappears in the alcohol rich systems when the eutectic transition goes below 64 °C. The apparent increase in the melting temperature of the high alkane model waxes is due to peak broadening causing difficulties in assigning exact transition temperatures, most likely caused by kinetic effects in the sample. Effects of surfactants on aqueous dispersions of the model wax (*i.e.* 1, 4, or 25 % in $C_{22}H_{45}OH/C_{32}H_{66}/H_2O$: 40/10/50 and 10/40/50). DSC results are shown in figure 23. The melting endpoint decreases by ≤ 1.2 and ≤ 0.3 °C for $C_{10}EO_7$ and $C_8G_{1.6}$ respectively, and the eutectic transition line decreases by 1.0 °C for both surfactants. Both $C_{10}EO_7$ and $C_8G_{1.6}$ cause a minor increase in the alcohol hydrate formation temperature, while no effect is seen on the alkane rotator transition. X-ray diffraction (SWAXD) shows no effect on wax crystal structure upon water and surfactant exposure (data not

shown). Figures 22-23 show the effects on phase transition temperatures from adding one of the compounds $C_{10}EO_7$, $C_8G_{1.6}$, or tebuconazole to the model wax. Of these three, tebuconazole had the most pronounced effect, followed by $C_{10}EO_7$ and $C_8G_{1.6}$. $C_{22}H_{45}OH$ showed a stronger response to the added substances than $C_{32}H_{66}$, and while the transition temperatures were generally lowered for the alcohol, they were largely unaffected for the alkane. Adding a third component to the model wax also lowers the eutectic point and the temperature change is dependent on the ability of the components to mix in the melted state. This explains the change seen with tebuconazole, $C_{10}EO_7$, and $C_8G_{1.6}$ in figures 22-23, as tebuconazole is the most hydrophobic of the three. If mole fractions are considered, instead of mass fractions, these effects are retained in the same order although the differences are slightly less pronounced. Both surfactants caused a marginal decrease in eutectic transition and end point of melting of the wax in the wet state (about 1 °C), but they are most probably caused by kinetic effects due to separation of hydrophobic domains in the sample.

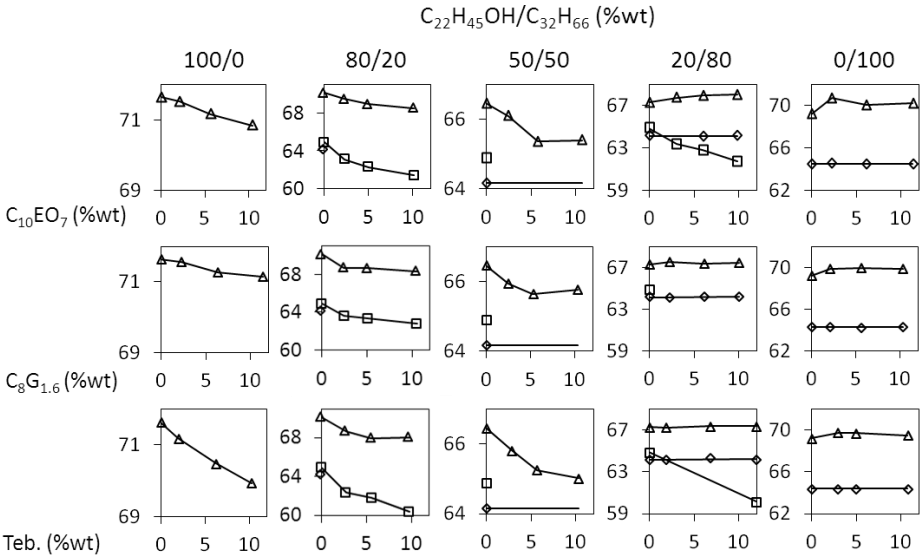

Figure 22. *Effect of $C_{10}EO_7$, $C_8G_{1.6}$, or tebuconazole on phase transition temperatures of model wax mixtures ($C_{22}H_{45}OH/C_{32}H_{66}$: 100/0, 80/20, 50/50, 20/80, 0/100). Data points; Triangles: Endpoint of melting, Squares: System Eutectic, Rhombi: $C_{32}H_{66}$ rotator transition. X-axis: %wt added substance, Y-axis: Temperature (scaled for clarity).*

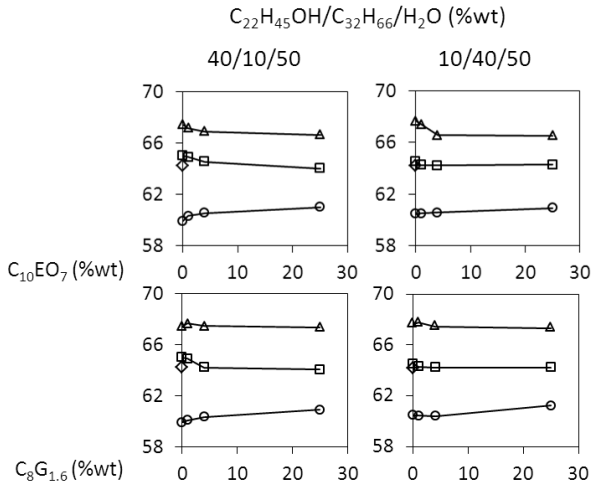

Figure 23. *Effect of $C_{10}EO_7$ or $C_8G_{1.6}$ on phase transition temperatures of water/model wax mixtures ($C_{22}H_{45}OH/C_{32}H_{66}/H_2O$: 40/10/50, 10/40/50). Data points; Circles: hydrate formation, Rhombi: $C_{32}H_{66}$ rotator transition, Squares: System Eutectic, Triangles: Endpoint of melting. X-axis: %wt added substance (dry mass), Y-axis: Temperature.*

Surfactant induced changes in cuticle model wax II: Fluidity

Cuticle wax surfactant absorption caused changes in the phase transition temperatures of the model wax, as seen above. These results add to the understanding of the effects the interaction between cuticle wax and surfactant may present. However, the barrier properties of the cuticle are also related to the softness of the cuticle **[8]**. Thus, how surfactants affect the softness – or fluidity – of the model wax can offer some deeper insight in surfactant – cuticle interactions. QCM-D was employed to investigate this.

Continuous QCM-D experiments

Model wax films were prepared on QCM-D sensors and surfactant effects on the rheological properties of these films were quantified. Aqueous solutions of $C_{10}EO_7$ and $C_8G_{1.6}$ (i.e. 1, 4, or 25 % (aq)) were evaluated. QCM-D measures how the oscillating frequency changes as the total mass of sensor and film vary, *i.e.* a high mass lowers the sensor oscillation frequency. The technique also measures the ability of the film covered sensor to continue to oscillate as the power input is discontinued; this is called the dissipation of the adsorbed film. A higher dissipation means a less rigid film. All QCM-D experiments were performed at a controlled temperature of 25 °C.

Surfactant adsorption and desorption to clean gold sensors were recorded as the baseline (data in Paper III). The frequency and dissipation shifts over the sequence of liquids starting from water followed by: 1 % surfactant solution, water, 4 % surfactant solution, water, 25 % surfactant solution and water. After water rinsing, the residual changes in frequency and dissipation were insignificant compared to the clean sensor. This indicates that negligible amounts of surfactants remain at the sensor surface. The sensors got a frosty appearance and a thin film could be appreciated after deposition of model waxes ($C_{22}H_{45}OH/C_{32}H_{66}$, 80/20 or 20/80). Heat treatment made the film more compact and evenly distributed over the gold surface, which was confirmed by AFM (data not shown). The average (n=6) thickness, shear viscosity, shear elastic modulus and G''/G'-ratio of the spin-coated films were determined in air employing the Kelvin-Voigt model (Paper III). The effects on frequency and dissipation of 1% surfactant solutions ($C_{10}EO_7$ or $C_8G_{1.6}$, aq) on the two wax films were evaluated in triplicate. Adding surfactants caused the frequency to drop sharply and the dissipation rose, indicators of increased mass and a less stiff film. However, the frequency quickly increased again and the dissipation decreased, indications of film thinning, i.e. wash-off.

Pulsed QCM-D experiments

A pulsed QCM-D experiment was designed to evaluate the effects that surfactants have on the spin-coated wax film without removing substantial amounts of material from the surface. Unlike the previous continuous QCM-D experiment, the spin-coated wax films were now only exposed to short pulses of surfactant solution. The surfactant concentration in the solution was increased stepwise and the experiments were performed in triplicate. A characteristic response in frequency- and dissipation shifts is presented in figure 24. The first plateau in the curve represents the wax covered gold sensor in water, followed by a 20 s pulse of 1 % surfactant solution, sensor in water, a 20 s pulse of 4 % surfactant solution, sensor in water, a 20 s pulse of 25 % surfactant solution and sensor in water. The surfactant pulses induce a decrease in frequency and an increase in dissipation. After this peak effect of the surfactant pulses the dissipation levels off at a higher value for each step indicating a stepwise less rigid film. The frequency curves level off at lower values for the first and second exposure, indicating a larger sensed mass, and at a higher value for the final pulse, indicating a minor wash-off.

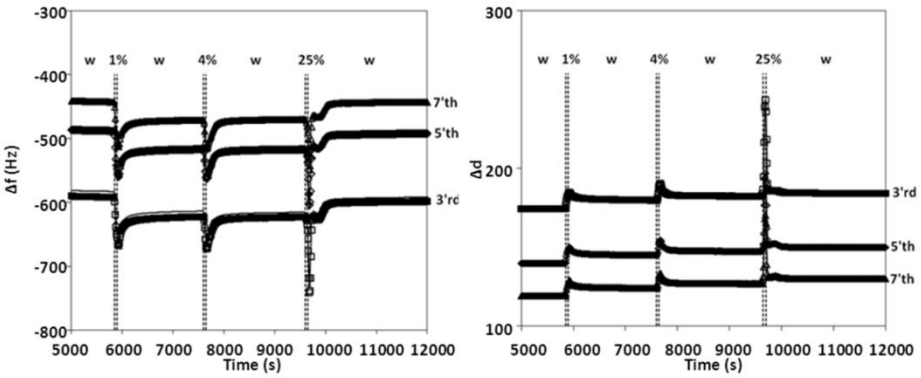

Figure 24. *Characteristic frequency and dissipation change -plot from water and $C_{10}EO_7$ (aq) treatment of model $C_{22}H_{45}OH/C_{32}H_{66}$: 80/20 wax vs time, pulsed QCM-D experiment. Data points: Squares, Rhombi, and Triangles, corresponds to the 3'rd, 5'th, and 7'th overtone respectively. Lines fitted using Q-tools.*

Changes in the modelled parameters during the experiment are displayed in figure 25. All changes in frequency and dissipation along with the values for the modelled parameters are listed in Paper III. As shown in figure 25, the shear elastic modulus drops sharply when a surfactant pulse is introduced to the system and it recovers to some degree when water is again the medium. The film thickness increases rapidly on surfactant addition and then decreases, while the shear viscosity of the film has a sharp prevailing increase. Thus the parameters change in irreversible steps triggered by the surfactant pulses throughout the experiment. The change in G''/G' in the same experiment is also shown in figure 25. The wax film in water has a stable G''/G' ratio around 0.15, but when the surfactant solutions are pulsed through the system this ratio increases in steps with each pulse. The 1, 4, and 25 % pulse increases the G''/G' ratio to approximately 0.18, 0.22, and 0.27, respectively. Water rinsing between the pulses did not alter the G''/G' ratio. The relative change in the G''/G'-ratio for each surfactant-wax combination was evaluated by setting the G''/G' ratio for the water plateau prior to surfactant exposure equal to 1. The G''/G' ratio at the water plateaus after each consecutive surfactant pulse were compared to the original value and a relative change could be obtained. In figure 26 the effect of the two surfactants on model wax surfaces are compiled for the pulsed QCM-D experiments. The strongest effect is seen with the combination of the $C_{10}EO_7$ surfactant and the $C_{22}H_{45}OH$/ $C_{32}H_{66}$ 80/20 model wax, and the second strongest effect is seen with the same surfactant

and the $C_{22}H_{45}OH$/ $C_{32}H_{66}$ 20/80 model wax. A maximum relative increase of approximately 1.8 and 1.2 times, respectively, is observed after the 25 % surfactant solution pulse. In the same set of experiments, the other surfactant, $C_8G_{1.6}$, causes a decrease in the relative G''/G' ratio. This effect is more pronounced with higher surfactant concentration. $C_8G_{1.6}$ in combination with the $C_{22}H_{45}OH$/ $C_{32}H_{66}$ 80/20 and the $C_{22}H_{45}OH$/ $C_{32}H_{66}$ 20/80 model wax gives relative values for the G''/G' ratio of approximately 0.9 and 0.8 respectively, after the 25 % surfactant solution pulse.

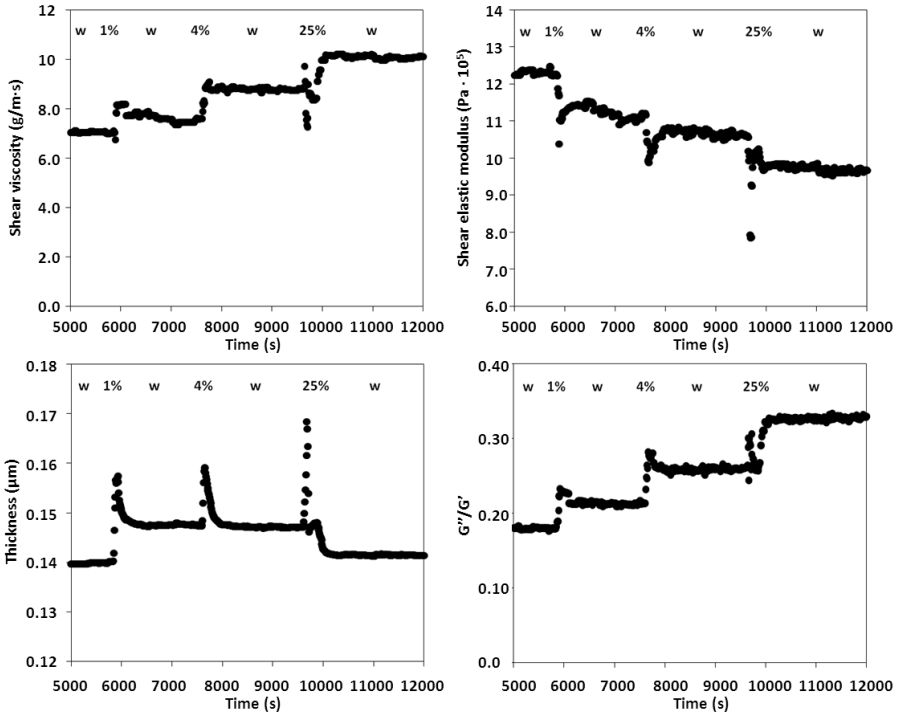

Figure 25. *Characteristic plot over changes in modelled parameters (shear viscosity, shear elastic modulus, thickness, G''/G') from water and $C_{10}EO_7$ (aq) treatment of model $C_{22}H_{45}OH/C_{32}H_{66}$: 80/20 wax vs time, pulsed QCM-D experiment.*

A control experiment was also performed where the mass of wax on the sensor was compared before and after 1 and 4 % surfactant exposure; after each pulse the frequency and dissipation return to their start values prior to surfactant exposure.

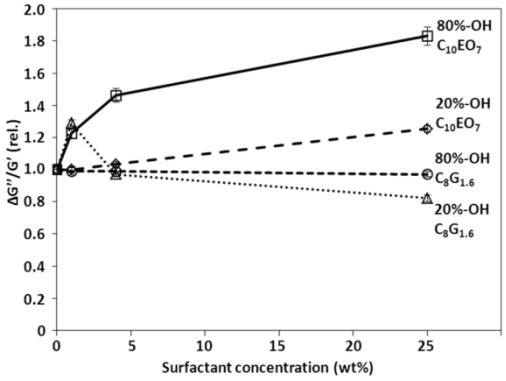

Figure 26. *Relative changes compared to the original G''/G' ratio for each surfactant-wax combination. G''/G' plot vs increasing surfactant concentrations, pulsed QCM-D experiment. Data from water plateaus between the surfactant peaks (n=3). Squares ($C_{22}H_{45}OH/C_{32}H_{66}$: 80/20, $C_{10}EO_7$), Circles ($C_{22}H_{45}OH/C_{32}H_{66}$: 80/20, $C_8G_{1.6}$), Rhombi ($C_{22}H_{45}OH/C_{32}H_{66}$: 20/80, $C_{10}EO_7$), Triangles ($C_{22}H_{45}OH/C_{32}H_{66}$: 20/80, $C_8G_{1.6}$).*

Wax film rheology

QCM-D was employed to quantify the effects that $C_{10}EO_7$ and $C_8G_{1.6}$ have on the change in frequency and dissipation of oscillating sensors, clean or covered by a film of model wax in two different compositions. The temperature was 25 °C in all experiments. Wax films in water have a shear elastic modulus (μ_f or G´) between $1x10^6$ and $2x10^6$ Pa, and a shear loss modulus (G") of around $2x10^5$ Pa. Severtson and Nowak report G' and G" of pure C_{21} and C_{23} alkanes to be around $5x10^7$ and $7x10^6$ Pa, respectively, and around $3x10^7$ and $5x10^6$ Pa respectively for a mixture **[95]**. They also report G' and G" values for a commercial paraffin wax (a mixture of C_{18}-C_{40} alkanes, centred at C_{23}) to be around $3x10^7$ and $3x10^6$ Pa, respectively **[96]**. Lionetto and co-workers report waxy crude oil to have a shear elastic modulus of around $1x10^5$ and a shear loss modulus of around $1x10^4$ **[97]**. These determinations were however done at much lower frequency (1 Hz) than that employed in QCM-D here (around 4.95 MHz). The experiments on clean sensors revealed that $C_{10}EO_7$ induces a larger change in both frequency and dissipation than $C_8G_{1.6}$. This can be explained by the size and structure of the two molecules. $C_{10}EO_7$ has a larger molecular mass and is less bulky than $C_8G_{1.6}$; $C_{10}EO_7$ also diffuses more rapidly to the surface especially at higher concentrations. Hence, more molecules of the former surfactant can adsorb per unit area, which results in a larger sensed mass. Surfactant concentrations are above CMC for all cases except 1%

$C_8G_{1.6}$, but this does not mean that the change in bulk viscosity with surfactant concentration and its effect on frequency and dissipation data can be neglected **[98]**. The continuous experiments on wax covered sensors (Paper III) showed that the response of model wax surfaces to surfactant exposure is rather fast. Within a couple of minutes drastic effects were observed, inevitably leading to wash-off. After an initial decrease following exposure, the frequency increased by 250 Hz for all of the overtones shown (3, 5 and 7). Thus the surfactants remove wax from the surface. The main idea of doing the pulsed set of experiments was to study the effect of surfactant solutions of different concentrations (1, 4, and 25 %) on the wax films, as well as to observe the relaxation when going from bulk surfactant solution back to water - i.e., to evaluate the reversibility of the surfactants effect on the wax films. The pulsed type of experiment was also a way to avoid effects on Δf and ΔD from changes in bulk properties and to reduce wax wash-off caused by the surfactant. Wash-off is promoted by exposure time, energy, temperature, and surfactant concentration. Reducing exposure time from 40-90 minutes to just 20 seconds and varying the surfactant concentration in the pulses proved to reduce wash-off substantially and allowed for surfactant effects to be quantified in more detail. This experimental setup is kinetically controlled (it is dependent on the diffusion coefficients of the surfactants in water and wax), and 20 seconds was deemed to be sufficient to allow surfactants to affect the surface while at the same time keeping wash-off minimal. As for the continuous QCM-D experiments the wax responds to surfactant exposure rather rapidly. In figure 25 the stepwise change in the modelled parameters can be observed. Compared to the frequency and dissipation plots in figure 24, it is clear that the effect of the surfactant does not diminish after the surfactant pulse. Instead the effect prevails for at least 30 minutes after just 20 seconds of possible absorption and hence G''/G' is constant during water rinse periods. A stepwise and irreversible (during the current time-scale) softening of the film can be observed after every consecutive pulse. At the 25 % surfactant pulse wash-off can in fact be seen, although not very severe since the frequency correlates to that of the first water period. The control experiment revealed that the change in mass before and after surfactant exposure (1 %, or 1 % followed by 4 %) is negligible. Furthermore, the fact that dissipation and frequency return to their initial values after the pulses, indicates that the effects seen in water plateaus in between the pulses are not caused by increased surface roughness. If the roughness had increased, more water would be dragged along the oscillating surface, which would show up as an apparent decrease in frequency.

The changes seen in the frequency and dissipation as well as the changes in the modelled parameters (shear viscosity, shear elastic modulus, thickness, and G''/G') cannot be explained by simple surfactant adsorption. If that would be the case, the frequency and dissipation would go back close to their initial values (± the small changes shown in the results for clean sensors) for water in between the surfactant pulses. But this does not happen and thus the surfactant also absorbs in the film and affects its fluidity. Even at this rather short-pulse treatment a large amount of the $C_{10}EO_7$ surfactant seem to be trapped inside the alcohol dominated wax film as the fluidity continues to increase with each step. Also, $C_{10}EO_7$ has a small fluidizing effect on the alkane rich film as well. At low concentrations and short exposure times $C_8G_{1.6}$ has an effect on fluidity of the high alkane model wax, however at higher concentrations this surfactant tends to solidify both types of wax films. This is probably due poor absorption of $C_8G_{1.6}$ into the film, being bulkier and considerably more hydrophilic, and also less surface active. The reason for the rather strong effect seen in these experiments could be that the wax film is formed from smaller crystalline domains (Fig. 27).

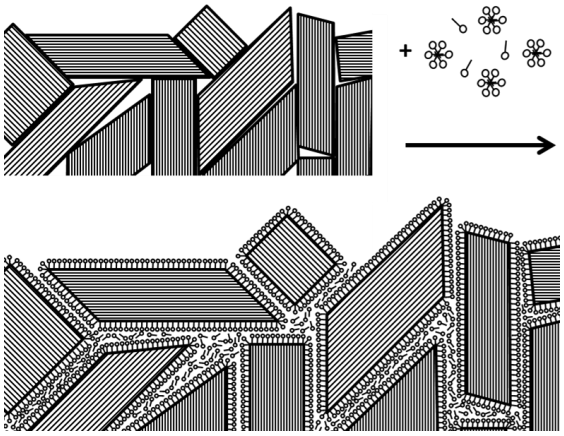

Figure 27. *Schematic overview of surfactant absorption and entrapment in between crystalline wax domains.*

X-ray diffraction (SWAXD) experiments did not reveal any influence of water and/or surfactant on the model wax crystal structure within these domains. However, surfactant and water may enter the crevices (or grain boundaries) between the individual domains to separate them through a continuous less ordered wax/water/surfactant network. The alcohol dominated wax should be more prone to such effects as it is less hydrophobic than the wax dominated by the alkane. Even in the absence of water $C_{10}EO_7$ has a fluidizing effect on wax (Fig. 22, **[81]**), although the effect is stronger with water. The mechanism

of surfactant/water absorption in crevices between crystalline wax domains is supported by the observation that the G''/G' ratio does not decrease even after the surfactant addition to the system is discontinued.

Diffusion in the cuticle

Up to this point the focus has been on cuticle characteristics, cuticle model wax, properties of surfactant solutions, surfactant/cuticle interaction and surfactant/model wax interaction. What these investigated changes do to the actual transport of an AI over the cuticle still remains to be investigated. How two selected surfactants change the flux of a model AI over intact *Clivia* leaf cuticle was evaluated using Franz diffusion cell equipment.

Cuticle membrane

Plant leaf cuticle membranes were obtained from the stomata free **[99]** upper side of Clivia leaves, using either a dermatome (CM-d, details in Paper IV) or a previously established enzymatic isolation technique (CM-e) **[56]**. No visible damage to dermatomed cuticles could be seen in SEM experiments. The two different isolation techniques proved to give membranes of very similar characteristics in terms of permeability. However, the degree of leaf maturation had a drastic effect on tebuconazole cuticle diffusion (details in Paper IV). All membranes for further experiments were therefore retrieved mid-leaf. The approach in this work, where CM-d specimens were used as membranes and HPLC-UV was employed to assay solute transport across membranes, enables the quantification of solute transport over plant leaf CM without the need for enzymatic cuticle separation and radiolabeled solutes. This streamlined and less cumbersome protocol should be universally applicable to flat leaves of sufficient size and thickness, tentatively at least: 60x30x0.2 (length x width x thickness, mm).

Membrane partition

As mentioned in the experimental part of this thesis, partition of a substance is important to know when investigating its transport over a membrane. To determine how the solute tebuconazole partitions between the particular membrane material and the surrounding, solution sorption isotherms were obtained. The silicone tebuconazole sorption isotherm was fitted to a non-linear GAB (Guggenheim-Anderson-de Boer) model **[100, 101]** (Fig. 28A), while the CM-e sorption isotherm was best fitted to a linear model (Fig. 28B), they correspond to approximately: log $K_{s/w} \approx 1.40$ (silicone/water) and log $K_{c/w} = 2.95$ (CM/water), c.f. log $K_{c/w} = 3.54$ **[8]**.

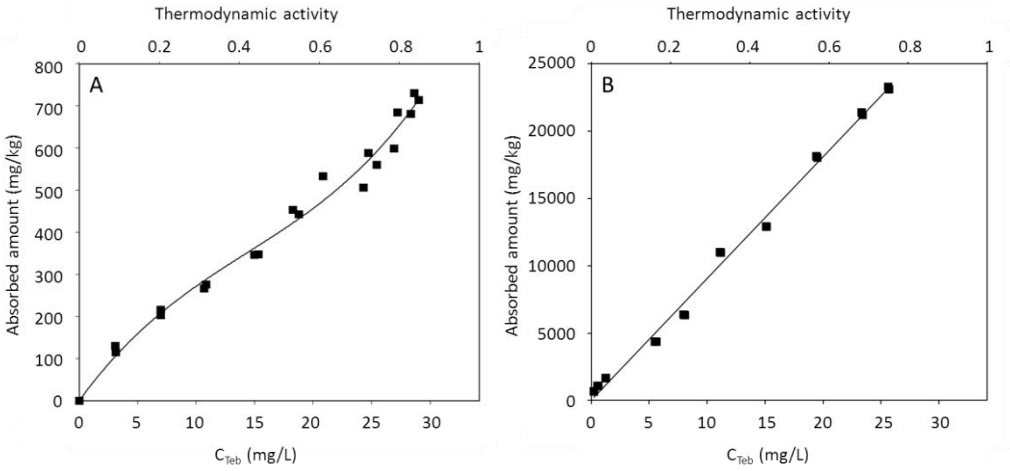

Figure 28. *A: Sorption isotherm of tebuconazole in silicone (fitted to a non-linear GAB model), B: Sorption isotherm of tebuconazole in CM-e (fitted to a linear model).*

Membrane permeability

The flux over the non-responding silicone membranes was mainly governed by the thermodynamic activity, *vide supra*. Tebuconazole permeability over Clivia CM was evaluated with the same set of test formulations as used for silicone (Paper IV for details). Formulations containing surfactant significantly shortened the lag-times; formulations with identical thermodynamic activity performed as $C_{10}EO_7$ > $C_8G_{1.6}$ > pure water. $C_{10}EO_7$ and $C_8G_{1.6}$ produced steady-state fluxes 4 and 3 times higher than water, respectively (Fig. 29). Clearly, it appears that both surfactants affect the cuticle to increase the diffusion coefficient (D_i) of tebuconazole therein.

Solute distribution and diffusion

The diffusion experiments had initially fixed boundary conditions (i.e., fixed concentration or fixed thermodynamic activity of the solute in the donor formulation). Even so, the distribution of solute over the different compartments (donor, membrane and receptor) will change with time. The sorption isotherms (Fig. 28) and diffusion experiment data were employed to calculate the distribution profile of two carrier formulations and how the profile changes during the course of the experiment. This was done for both silicone and CM membranes and is presented in figure 30.

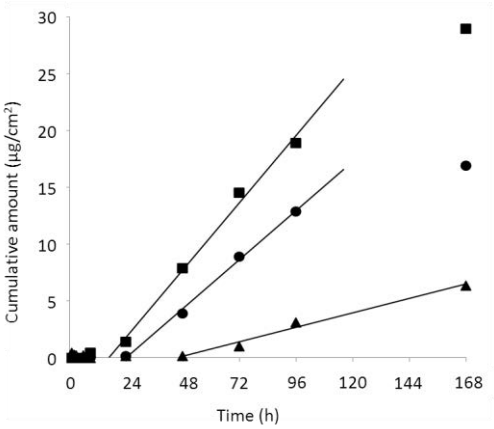

Figure 29. *Steady-state flux $C_{10}EO_7$ (Squares), $C_8G_{1.6}$ (Circles), and water (Triangles) formulations of 0.8 tebuconazole saturation concentration over cuticle membranes.*

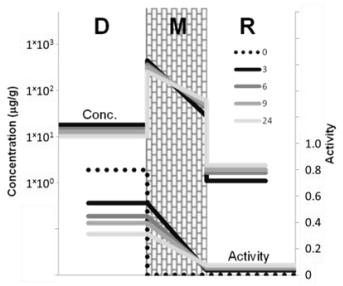

A: 26 mg/L in H_2O, Silicone

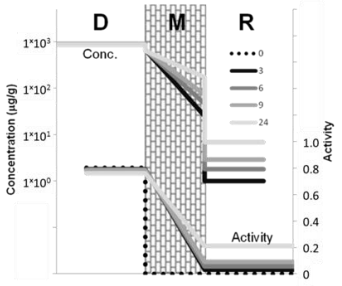

B: 911 mg/L in 4% $C_{10}EO_7$(aq.), Silicone

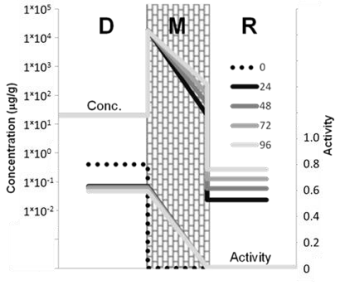

C: 26 mg/L in H_2O, Ez *Clivia*

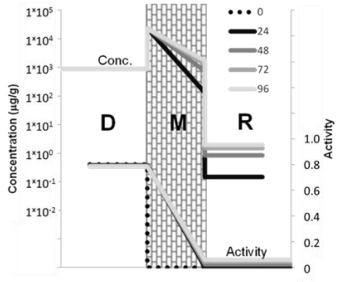

D: 911 mg/L in 4% $C_{10}EO_7$(aq.), *Clivia*

Figure 30. *Changes in tebuconazole distributions profiles over donor-, membrane-, and receptor compartments comprising the diffusion cell vs. time. Left to right in each figure: donor-, membrane-, and receptor compartment, left y-axis: concentration, and right y-axis: thermodynamic activity. Top: Silicone-, bottom: CM. Left: H_2O 26 mg/L, CM-e, right: 4% $C_{10}EO_7$(aq), CM-d, 911 mg/L carrier formulation.*

In the silicone experiments, 26 mg/L in H_2O, the thermodynamic activity of tebuconazole decreases rapidly in the donor formulation from 0.8 to about 0.3 after 24h. This shows that the donor formulation needs to be replaced regularly during the experiment to maintain steady-state flux. Sink conditions in the receptor compartment are well preserved (i.e. $a_{teb} < 0.1$) **[102]**. With the 911 mg/L in 4% $C_{10}EO_7$(aq) formulation steady-state conditions are reasonably well preserved over the first 9 hours. Sink conditions in the receptor compartment are violated (i.e. $a_{teb} > 0.2$) at 24 hours and thereby the gradient in thermodynamic activity over the membrane is diminished. For Clivia membranes an initial decrease in donor solute activity is observed (to approx. $a_{teb} = 0.6$) before apparent steady-state conditions are obtained for the 26 mg/L in H_2O formulation. This fact may be attributed to the ability of the CM to accommodate large amounts of tebuconazole. The donor solute activity remains almost constant for the 911 mg/L in 4% $C_{10}EO_7$(aq) formulation and sink conditions in the receptor compartment are well preserved (i.e. $a_{teb} < 0.1$) for both formulations. Up to this point the focus has been on tebuconazole flux and compartment distribution as a function of the gradient in thermodynamic activity over the membrane, with or without surfactants present. However, the results clearly show (Fig. 29) that surfactants also may affect the diffusivity of tebuconazole within the membrane, as reflected by the diffusion coefficient (D_i) (c.f. Ficks law, Eq. 1). Schreiber and Schönherr **[8]** reviewed alternative methods for determining the diffusion coefficient in plant CM based on permeation data. Two of these methods were adopted as examples and are shown below (Eq. 10 and Eqs. 11-12, respectively). Equation 10 used the extrapolated lag time (t_e) and the square of the membrane thickness (z^2):

$$D_i = \frac{z^2}{6t_e}$$

(Eq. 10)

The second method is based on the fraction of tebuconazole permeated (m^r/m^t) *vs* the square root of time. The slope (Eq. 12) is generated from $m^r/m^t \in \sqrt{t}$:

$$\frac{m^r}{m^t} = \frac{4}{\sqrt{\pi}}\sqrt{\frac{Dt}{z^2}}$$

(Eq. 11)

$$D = \frac{\pi(slope)^2 z^2}{16}$$

(Eq. 12)

Both methods are commonly used, although when applied to the current data set they generate diffusion coefficients that differ by several orders of magnitude (details in Paper IV). According to our knowledge there are no data on diffusion coefficients for tebuconazole in Clivia leaf CM available from the literature. However, related data may be used for comparison: 2,4-D (2,4-dichlorophenoxyacetic acid) diffusion in reconstituted cuticle wax from barley (1.9×10^{-17} m^2/s) **[94]** (calculated using Eq. 11-12), and in Clivia (2.2×10^{-16} m^2/s) **[103]** (Eq. 10), as well as tebuconazole in reconstituted cuticle wax from barley (5.8×10^{-18} m^2/s) **[94]** (Eq. 11-12). To resolve the apparent discrepancy between the diffusion coefficients calculated using the two methods above a third method was derived in Paper IV. This method is based on Fick's first law (Eq. 1) and does not require steady-state conditions or refilling of donor compartment to function properly. The sorption isotherm of the solute is assumed to be linear i.e. that partition coefficients and the solute thermodynamic activity in solution may be used to set the concentration of the solute in the membrane. Furthermore, the profiles of the solute concentration and the thermodynamic activity gradient in the membrane are both assumed to be linear. When this is applied to Fick's first law (Eq. 1), Equation 13 can be derived to describe how the mass of solute in the receptor compartment changes with time (dm^r/dt):

$$\frac{dm^r}{dt} = -\frac{ADK_{cw}}{C^0}\frac{\Delta C}{dz} = -\frac{ADK_{cw}}{C^0 \Delta z}\left(\frac{m^r}{V^r} - \frac{m^d}{V^d}\right)$$

(Eq. 13)

A is the area of the membrane, D is the diffusion coefficient, K_{cw} is the membrane/surrounding liquid partition coefficient (obtained using the sorption isotherms in figure 28 for the silicone membrane and the Clivia CM-e), C^0 is the saturation concentration of the active ingredient at a given surfactant concentration (obtained through the solubility curve in figure 19), and Δz is the thickness of the membrane. m^d and m^r are the solute mass in the donor and receptor compartments of the diffusion cell, V^d and V^r are the corresponding volumes of these compartments. Since m^d is not known, Eq. 13 can be rearranged into the form of Eq. 14 that instead contains m^r and m^t (*i.e.* total mass of solute in the system), both of which are known.

$$\frac{dm^r}{dt} = a(cm^t - bm^r)$$

(Eq. 14)

Three coefficients (a, b and c) are used in Eq. 14, outlined in Eqs. 15-17 (V^m is the volume of the membrane):

$$a = \frac{ADK_{cw}}{C^0 \Delta z}$$

(Eq. 15)

$$b = \frac{1}{V^r} + \frac{\left(1 + \frac{V^m K_{cw}}{V^r 2C^0}\right)}{V^d \left(1 + \frac{V^m K_{cw}}{V^d 2C^0}\right)}$$

(Eq. 16)

$$c = \frac{1}{V^d \left(1 + \frac{V^m K_{cw}}{V^d 2C^0}\right)}$$

(Eq. 17)

Integrating Eq. 14 with respect to time gives Eq. 18, while Eq. 19 is a reorganization of Eq. 18. Plotting the left side of Eq. 19 vs Δt (the time past lag time, $\Delta t = t - t_c$) generates a slope (-ab), from which the diffusion coefficient (D) is derived by employing Eq. 15 and Eq. 16. Eq. 19 can be used to predict solute flux at any given D.

$$\ln(cm^t - bm^r) - \ln(cm^t) = -ab\Delta t$$

(Eq. 18)

$$m^r = \frac{cm^t(1 - \exp(-ab\Delta t))}{b}$$

(Eq. 19)

The first method (Eq. 10) and third method (Eqs. 14-19) produce similar diffusion coefficients, while the second method (Eqs. 11-12) suffers from the facts that the amounts of solute present inside the membrane itself, and the gradient in solute chemical potential are neglected. The third method takes this into account and shows a more consistent effect from surfactant addition, i.e. a 3-14 times increase in D. At fixed tebuconazole concentration (26 mg/L), $C_{10}EO_7$ is superior to $C_8G_{1.6}$ (i.e. 14x and 4x vs. the water carrier), while at fixed thermodynamic activity (a_{teb}=0.8) the surfactants generate an increase in D by roughly 4 and 3 times, respectively. In addition, Burghardt and co-workers report an increase of the diffusion coefficient for tebuconazole in re-

constituted barley (Hordeum) leaf waxes by about 9 times when $C_{12}EO_8$ is present **[94]**. The $C_{10}EO_7$-formulation does however carry 5 times more tebuconazole compared to the $C_8G_{1.6}$-formulation and thus the smaller increase in D at higher solute concentration may be attributed to a crowding effect at high concentrations. The limited space available for diffusion in the dense CM is in this case not sufficient to allow for all tebuconazole molecules to diffuse unhindered at maximum individual rate. Thus, the less pronounced increase in diffusion coefficients observed at higher solute concentrations could be qualitatively explained, as previously discussed by e.g. Baur and co-workers **[104]**. Such crowding effects are not observed in silicone membranes, see figure 20, owing to the limited partition of tebuconazole to the silicone membrane, in comparison to the Clivia CM (Fig. 29). With reference to Eq. 1 the flux (J_i) depends solely on D_ic_i at a constant thermodynamic activity gradient (da_i/dt) and barrier thickness (z). Furthermore, the same quantitative increase in both J_i and D_i was observed in the presence of surfactants. Therefore it may be concluded that both $C_{10}EO_7$ and $C_8G_{1.6}$ induce changes in the barrier properties, which affects the solute mobility (D_i) in the cuticle while leaving the solute concentration inside the membrane (c_i) unchanged. Thus, the CM-water partition coefficient ($\lg K_{cw}$) is not affected by either of the two surfactants and the sorption isotherm presented based on thermodynamic activity is valid for all formulations. In the calculations of diffusion coefficients the CM was considered to be homogenous with a single D to describe the solute diffusion. However, the cuticle is indeed heterogeneous **[8]** and partition-, and diffusion coefficients vary between different compartments within the membrane. Since the exact structure of the cuticle is not known, an average thickness of 8.5 μm was used to calculate D, (c. f. Fig 6D and **[8 p.44]**).

CONCLUDING REMARKS AND FUTURE OUTLOOK

In this work the following topics have been addressed: cuticle characteristics, properties of a cuticle model wax, surfactant solution characteristics, surfactant/cuticle interactions, surfactant/model wax interactions, and diffusion through the cuticle. The cuticle is the main barrier to solute penetration and intact sliced plant leaves can replace enzymatically isolated cuticles in the evaluation of in vitro permeability of solutes. However, the barrier function of the Clivia CM improves with maturation of the leaf and membranes for in vitro studies should thus be harvested mid-leaf. The native Clivia cuticle wax is heterogeneous and contains both crystalline and amorphous domains. The wax has a broad melting interval between 40 and 80°C which comprises a crystalline transition from orthorhombic to hexagonal sub-cell. This transition is facilitated by addition of surfactants. Both intact cuticle and extracted wax also possess lamellar long range order. *Clivia* is an appropriate model plant since it is related to some of the most important crop plants, wheat and barley, and has similar leaf characteristics. It is easy to cultivate indoors and the leaves are wide enough to be evaluated *in vitro* through diffusion cell experiments. The barrier is very tough; if it works on *Clivia* it most probably will work in the field as well. A model of plant leaf intracuticular wax can be used to estimate formulations effects on the cuticle structure. The model was based on leaf wax extract and included 1-docosanol ($C_{22}H_{45}OH$) and dotriacontane ($C_{32}H_{66}$). The thermotropic phase behaviour of the model was investigated, and the structure of individual phases in the model wax - water system was determined. The thermotropic transitions of the model wax fit in the window of the extracted leaf waxes, but the model wax would benefit from further development, striving for a more amorphous system.

The effects of surfactants on the phase behaviour and the rheological characteristics of the model wax were quantified. This was done to address the current lack of understanding of how surfactants affect the barrier properties of plant leaf cuticles on a molecular level. The model wax used is crystalline at ambient conditions, yet it is clearly softened by the surfactants. The softness of the wax film increased in irreversible steps after surfactant exposure and $C_{10}EO_7$ has a stronger fluidizing effect than $C_8G_{1.6}$. Intracuticular waxes (IW) comprise both crystalline and amorphous domains. Surfactants exercise their fluidizing effects in amorphous regions. A mechanism is suggested to explain the fluidizing effects seen on a primarily crystalline wax. It is proposed that surfactants may enter the crevices in between crystalline domains to establish an expanded continuous amorphous network. Surfactants allow higher amounts of AI in solution, *i.e.* AI available for penetration. Commercial products may contain such high amounts of AI that complete solubilisation of AI is never reached, even after dilution. Undissolved AI cannot enter the cuticle and may lead to an unnecessary environmental burden when dislocated from the leaf. The rate of AI leaf uptake may be increased by an appropriate surfactant. If the contents of surfactant and AI are set with care, penetration will increase and waste is decreased. Surfactants increase the flux of AI over the cuticle barrier by increasing the AI diffusion coefficient inside the cuticle. Based on Fick's first law, an algorithm that accommodates changes in boundary conditions and takes partition into account was developed. The new algorithm provides a more accurate method, compared to the standard equations normally used, for calculating solute diffusion coefficients in membranes. The same quantitative increase in both flux (J_i) and diffusion coefficient (D_i) was observed with surfactants present, while the CM-water partition coefficient (lg K_{cw}) remained unchanged.

By the establishment of QCM-D and membrane diffusion protocols and the investigations on model wax, a set of evaluation tools have been developed. These tools can facilitate the determination of desired properties of new and better adjuvants in agriculture. Subsequently, it may contribute to a more cost-efficient and environmentally friendly usage of pesticides in foliar spray applications. The wider aim of this project was to contribute to a more efficient and optimized pesticide application through investigation of the cuticle and its interplay with surfactant solutions. However, there are a number of paths to explore in order to further increase knowledge. To further characterize native leaf wax and perhaps even complete intact cuticle in terms of the thermotropic phase behaviour (by DSC) and rheological properties (by QCM-D), and to see

how those characteristics are affected by surfactants would put the understanding one step closer to the actual application. An interesting plant to evaluate in the context of further diffusion experiments would be wheat. It is one of the major sources for nutrition in the world today and susceptible to a number of devastating pests if untreated. Another fascinating path to go down is to continue the development of the model wax. This work might evolve to a powerful screening model for new pesticide formulations, and even in a greater distance to the construction of something that would resemble an artificial leaf. It is imperative that the work continues to improve the understanding of the surfactant/pesticide/plant reciprocity to enable optimization of pesticide usage. This ought to be a joint responsibility for both academic institutions and the agrochemical industry.

ACKNOWLEDGEMENTS

I am grateful to Federico Gomez (Lund University), Christy Whiddon (former AkzoNobel Surface Chemistry), Kåre Larsson (Camurus Lipid Research Foundation) and Peter Baur (former Bayer Crop Science) for valuable discussions and to Zoltan Blum, Jovice Bon Sing Ng, Peter Falkman, Justas Barauskas, and Sebastian Björklund (Malmö University) for technical assistance. Zoltan Blum is also highly acknowledged for linguistic advice. The Knowledge Foundation (Grant no. 2003/123), Gustaf Th Ohlssons Foundation, The Swedish Institute Visby Program, and Malmö University are thanked for financial support of the project.

I would like to thank my extraordinary wife Katja who always proofs to be my missing half - often more sensible yet even more passionate about life than me - and with who I have closely endured and enjoyed life as husband and Ph.D. student. My two utterly fantastic children Valter and Iris who can take Pappa back to ground and show him what really matters, constantly putting a smile on my face - challenging and fun in a way science can never become. I would also like to give thanks to my brother, John, my father, Lennart, and my mother, Annika, who stubbornly have supported me through this period of hardships and triumphs. I owe a very special thanks to my inspiring chemistry teachers ranging from upper secondary school, peaking in high school, and through University studies, the ones that got me onto this train in the first place. Peter, Karin, and Martina at AkzoNobel surface chemistry - Agro applications, that have proven to be very friendly and helpful as well as good scientists and project collaborators. Finally, my two very persistent supervisors at Malmö University: Johan and Vitaly. The two of you made this happen, you saw it through and pushed, supported, and contained me whenever it was needed – Thank you!

REFERENCES

1. United Nations, Department of Economic and Social Affairs, Population Division (2013). World Population Prospects: The 2012 Revision, Highlights and Advance Tables. Working Paper No. ESA/P/WP.228.
2. S. Bringezu, Towards sustainable production and use of resources: assessing biofuels. United Nations Environment Programme, Paris, France, 2009.
3. D. Tilman, K.G. Cassman, P.A. Matson, R. Naylor, S. Polasky, Agricultural sustainability and intensive production practices. Nature, 418 (2002) 671-677.
4. E.C Oerke, Crop losses to pests. J. Agr. Sci., 144 (2006) 31–43.
5. R.C. Gilden, K. Huffling, B. Sattler, Pesticides and Health Risks. JOGNN, 39 (2010) 103-110.
6. V.A. Hilder, D. Boulter, Genetic engineering of crop plants for insect resistance - a critical review. Crop Prot., 18 (1999) 177-191.
7. G.A. Matthews, Pesticide application methods. Blackwell Science, Oxford, UK, 2000.
8. L. Schreiber, J. Schönherr, Water and Solute Permeability of Plant Cuticles. Springer-Verlag Berlin Heidelberg, Germany, 2009.
9. A.K. Mohanty, M. Misra, L.T. Drzal, Natural Fibers, Biopolymers, and Biocomposites. CRC Press, Boca Raton, US, 2005.
10. Heredia, Biophysical and biochemical characteristics of cutin, a plant barrier biopolymer. Biochim. Biophys. Acta, 1620 (2003) 1 – 7.
11. Nawrath, Unraveling the complex network of cuticular structure and function. Curr. Opin. Plant. Biol., 9 (2006) 281–287.
12. H. Bargel, K. Koch, Z. Cerman, C. Neinhuis, Structure – function relationships of the plant cuticle and cuticular waxes – a smart material? Func. Plant Biol. 33 (2006) 893-910.
13. Ullmann's encyclopedia of industrial chemistry – waxes. Wiley-VCH Verlag, Weinheim, Germany, 2012.

14. H.J. Ensikat, M. Boese, W. Mader, W. Barthlott, K. Koch, Crystallinity of plant epicuticular waxes: electron and X-ray diffraction studies. Chem. Phys. Lipids, 144 (2006) 435-59.
15. 9th International Symposium on Adjuvants for Agrochemicals, ISAA Society; P. Baur and M. Bonnet, Eds.; August 2010, ISBN 978-90-815702.
16. 10th International Symposium on Adjuvants for Agrochemicals, ISAA Society; P. Castelani, D. Stock, and D. Puente Moran, Eds.; April 2013, ISBN 978-90-815702-0-6.
17. D.F. Evans, H Wennerström, The Colloidal Domain: Where Physics, Chemistry, Biology, and Technology Meet. pp. 195-198, Wiley-VCH, New York, USA, 657 1999.
18. C. Åberg, Steady-State Diffusion in Complex Amphiphilic Films. Dissertation Lund University, Lund, Sweden, 2009.
19. L. Schreiber, Review of sorption and diffusion of lipophilic molecules in cuticular waxes and the effects of accelerators on solute mobilities. J. Exp. Bot., 57 (2006) 2515–2523.
20. Buchholz, J. Schönherr, Thermodynamic analysis of diffusion of non-electrolytes across plant cuticles in the presence and absence of the plasticiser tributyl phosphate. Planta, 212 (2000) 103-111.
21. P. Baur, Mechanistic aspects of foliar penetration of agrochemicals and the effect of adjuvants. Recent Res. Dev. Agric. Food Chem., Trivandrum, India: Research Signpost (1998) pp. 809-839.
22. P. Baur, J .Schönherr, B. Grayson, Polydisperse ethoxylated fatty alcohol surfactants as accelerators of cuticular penetration. 2: Separation of effects on driving force and mobility and reversibility of surfactant action. Pestic. Sci., 55 (1999) 831-842.
23. P. Baur, B. Grayson, J. Schönherr, Polydisperse ethoxylated fatty alcohol surfactants as accelerators of cuticular penetration .1. Effects of ethoxy chain length and the size of the penetrants. Pestic. Sci., 51 (1997) 131-152.
24. L. Schreiber, K. Schorn, T. Heimburg, H-2 NMR study of cuticular wax isolated from Hordeum Vulgare L. leaves: identification of amorphous and crystalline wax phases. Eur. Biophys. J., 26 (1997) 371–380.
25. Buchholz, Characterization of the diffusion of non-electrolytes across plant cuticles: properties of the lipophilic pathway. J. Exp. Bot., 57 (2006) 2501–2513.
26. E.C. Reynhardt, M. Riederer, Structures and molecular-dynamics of plant waxes 2. Cuticular waxes from leaves of Fagus-Sylvantica L and Hordeum-Vulgare L. Eur. Biophys. J., 23 (1994) 59-70.
27. H. Ussing, The active ion transport through the isolated frog skin in the light of tracer studies. Acta Physiol. Scand. 17 (1949) 1–37.
28. T. Franz, Percutaneous absorption - relevance of in-vitro data. J. Invest. Dermatol. 64 (1975) 190–195.

29. R. Bronaugh, R. Stewart, Methods for invitro percutaneous-absorption studies 4: The flow-through diffusion cell. J. Pharm. Sci. 71 (1985) 64–67.
30. 1920 Nobel Prize in Chemistry Presentation Speech by G. de Geer.
31. Leo, C. Hansch, D. Elkins, Partition coefficients and their uses. Chem. Rev. 71 (1971) 252-616.
32. J. Crank, The mathematics of diffusion. Oxford Uni. Press, Oxford, UK, 1975.
33. M. Gibaldi, S. Feldman, Establishment of sink conditions in dissolution rate determinations – theoretical considerations and application to nondisintegrating dosage forms. J. Pharm. Sci., 56 (1967) 1238–1242.
34. P.L. Ritger, N.A. Peppas, A simple equation for description of solute release I. Fickian and non-fickian release from non-swellable devices in the form of slabs, spheres, cylinders or discs. J. Control. Release, 5 (1987) 23-36.
35. P. Costa, J.M. Sousa Lobo, Modeling and comparison of dissolution profiles. Eur. J. Pharm. Sci., 13 (2001) 123–133.
36. J. Siepmann, F. Siepmann, Modelling of diffusion controlled drug delivery. . Control. Release, 161 (2012) 351-362.
37. I.J. Bosman, S.R. Avegaart, A.L. Lawant, K. Ensing, R.A. de Zeeuw, Evaluation of a novel diffusion cell for in vitro transdermal permeation: effects of injection height, volume and temperature. J. Pharm. Biomed. Anal., 17 (1998) 493–499.
38. T.J. Halthur, T. Arnebrant, L. Macakova, A. Feiler, Sequential adsorption of bovine mucin and lactoperoxidase to various substrates studied with quartz crystal microbalance with dissipation. Langmuir, 26 (2010) 4901–4908.
39. G. Sauerbrey, Verwendung von schwingquarzen zur wagung dunner schichten und zur mikrowagung. Zeitschrift fur physik, 155 (1959) 206-222.
40. A.E.H. Love, A treatise on the mathematical theory of elasticity. 4'th ed., Dover Publishing, Mineola, N.Y, USA, 1944.
41. M.V. Voinova, M. Rodahl, M. Jonson, B. Kasemo, Viscoelastic acoustic response of layered polymer films at fluid-solid interfaces: Continuum mechanics approach. Phys. Scr. 59 (1999) 391-396.
42. L. Macakova, G.E. Yakubov, M.A. Plunkett, J.R Stokes, Influence of ionic strength changes on the structure of pre-adsorbed salivary films. A response of a natural multi-component layer. Colloids Surf. B, 77 (2010) 31–39.
43. J. Hamit Eminovski, Interactions of biopolymers and metal complexes at biological interfaces. Dissertation, Malmö University, Malmö, Sweden, 2011.
44. J. Engblom, On the phase behavior of lipids with respect to skin barrier function. Dissertation, Lund University, Lund, Sweden, 1996.
45. O. Glatter, O. Kratky, Ed., Small Angle X-ray Scattering. Academic Press, Waltham, US, 1982.
46. N. Ashcroft, D. Mermin, Solid State Physics Ch. 7, Thomson Learning, Stamford, US, 1976.

47. L. Wadso, N. Markova, A double twin isothermal microcalorimeter. Thermochim. Acta, 360 (2000) 101-107.
48. E.B. Sirota, H.E. King, D.M. Singer, H.H. Shao, Rotator phases of the normal alkanes: an X-ray scattering study. J. Chem. Phys. 98 (1993) 5809–5824.
49. V. Kocherbitov, A new formula for accurate calculation of water activity in sorption calorimetric experiments. Thermochim. Acta, 414 (2004) 43-45.
50. I. Wadso, L. Wadso, A new method for determination of vapour sorption isotherms using a twin double microcalorimeter. Thermochim. Acta, 271 (1996) 179-187.
51. F. Gerber, M. Krummenb, H. Potgeter, A. Roth, C. Siffrin, C. Spoendlin, Practical aspects of fast reversed-phase high-performance liquid chromatography using 3 μm particle packed columns and monolithic columns in pharmaceutical development and production working under current good manufacturing practice. J. Chromatogr. A, 1036 (2004) 127–133.
52. S. Masoum, H. Ghasemi-Estarki, H. Seifi, E.H. Ebrahimabadi, H. Parastar, Analysis of the volatile chemical constituents in Mindium laevigatum by gas chromatography — Mass spectrometry and correlative chemometric resolution methods. Microchem. J., 106 (2013) 276–281.
53. H.J. Ensikat, C. Neinhuis, W. Barthlott, Direct access to plant epicuticular wax crystals by a new mechanical isolation method, Int. J. Plant Sci. 161 (2000)143–148.
54. E.A. Baker, G. Hunt, P. Stevens, Studies of plant cuticle and spray droplet interactions: a fresh approach, Pest Manag. Sci. 14 (1983) 645–658.
55. J. Schönherr, M. Riederer, Foliar penetration and accumulation of organic chemicals in plant cuticles, Rev. Environ. Contam. Toxicol. 108 (1989) 1–70.
56. E. Chaumat, A. Chamel, Study of the cuticular retention and permeation of diuron using isolated cuticles of plants. Plant Physiol. Biochem., 28 (1990) 719–726.
57. R. Jetter, S. Schaffer, M. Riederer, Leaf cuticular waxes are arranged in chemically and mechanically distinct layers: evidence from Prunus laurocerasus L.,Plant Cell Environ. 23 (2000) 619–628.
58. C. Buschhaus, H. Herz, R. Jetter, Chemical composition of the epicuticular and intracuticular wax layers on adaxial sides of Rosa canina L. Leaves, Ann. Bot.-London 100 (2007) 1557–1564.
59. L. Schreiber, J. Schönherr, Mobilities of organic compounds in reconstituted cuticular wax of barley leaves: determination of diffusion coefficients, Pest Manag. Sci. 38 (1993) 353–361.
60. K. Koch, W. Barthlott, S. Koch, A. Hommes, K. Wandelt, W. Mamdouh, S. De-Feyter, P. Broekmann, Structural analysis of wheat wax (Triticum aestivum):from the molecular level to three dimensional crystals. Planta 223 (2006)258–270.

61. E.C. Reynhardt, M. Riederer, Structures and molecular dynamics of plant waxes. Eur. Biophys. J. 23 (1994) 59–70.

62. J. Sachleben, B. Chefetz, A. Deshmukh, P.G. Hatcher, Solid-state NMR characterization of pyrene–cuticular matter interactions. Environ. Sci. Technol. 38 (2004)4369–4376.

63. M. Dirand, M. Bouroukba, V. Chevallier, D. Petitjean, E. Behar, V. Ruffier-Meray,Normal alkanes, multialkane synthetic model mixtures, and real petroleumwaxes: crystallographic structures, thermodynamic properties, and crystallization. J. Chem. Eng. Data 47 (2002) 115–143.

64. S. Tsubaki, K. Sugimura, Y. Teramoto, K. Yonemori, J. Azuma, Cuticular membrane of *Fuyu* persimmon fruit is strengthened by triterpenoid nano-fillers. Plos one, 8 (2013) e75275.

65. D. Precht, Kristallstrukturuntersuchungen an Fettalkoholen und Fettsäurenmit Elektronen- und Röntgenbeugung II. Fett. Wiss. Technol. 78 (1976)189–192.

66. S. Fukushima, M. Yamaguchi, Interaction between higher alcohols and water, in: E. Matijevic (Ed.), Surface and Colloid Science, Springer-Verlag Berlin Heidelberg, Germany, 2001, pp. 33–34.

67. Métivaud, A. Lefevre, L. Ventola, P. Negrier, E. Moreno, T. Calvet, D. Mondieig, M.A. Cuevas-Diarte, Hexadecane (C16H34) + 1-hexadecanol (C16H33OH) binary system: crystal structures of the components and experimental phase diagram. Application to thermal protection of liquids. Chem. Mater. 17 (2005)3302–3310.

68. V. del Campo, E. Cisternas, H. Taub, I. Vergara, T. Corrales, P. Soza, Structure and growth of vapor-deposited n-dotriacontane films studied by X-ray reflectivity. Langmuir 25 (2009) 12962–12967.

69. D.L. Dorset, Chain length and the co solubility of n-paraffins in the solid state. Macromolecules 23 (1990) 623–633.

70. L. Messe, A. Perdigon, S.M. Clarke, A. Inaba, T. Arnold, Alkane/alcohol mixed monolayers at the solid/liquid interface. Langmuir 24 (2005) 5085–5093.

71. D. Small, The Physical Chemistry of lipids – From Alkanes to Phospholipids. Plenum Press, New York, USA, 1988.

72. E.S. Domalski, E.D. Hearing, Heat capacities and entropies of organic compounds in the condensed phase. Volume III. J. Phys. Chem. Ref. Data 25 (1) (1996).

73. G. Nichols, S. Kweskin, M. Frericks, S. Reiter, G. Wang, J. Orf, B. Carvallo, D. Hillesheim, J. Chickos, Evaluation of the vaporization, fusion, and sublimation enthalpies of the 1-alkanols: the vaporization enthalpy of 1-, 6-, 7-, and9-heptadecanol, 1-octadecanol, 1-eicosanol, 1-docosanol, 1-hexacosanol, and cholesterol at T = 298.15 K by correlation gas chromatography. J. Chem. Eng.Data 51 (2006) 475–482.

74. I.W. Schröder, Über die Abhängligkeit der Löslichkeit eines festen Körpers von seiner Schmelztemperatur. Zeitschrift f. physik Chemie, XI (1893) 449-465.

75. V. Kocherbitov, O. Söderman, L. Wadsö, Phase diagram and thermodynamics of the n-octyl beta-d-glucoside/water system. J. Phys. Chem. B 106 (2002)2910–2917.

76. J. Prausnitz, R. Lichtenthaler, E. de Azevedo, Molecular Thermodynamics of Fluid-Phase Equilibria. Prentice Hall PTR, New Jersey, USA, 1999.

77. B. Tong, Z.C. Tan, S.X. Wang, Thermodynamic properties of 1-docosanol. Phys. Chim. Sin. 24 (2008) 1699–1702.

78. S.S. Estrera, K.D. Luks, Partial miscibility behavior of the ethane + propane + n-dotriacontane mixture. J. Chem. Eng. Data 33 (1988) 350–354.

79. L. Schreiber, K. Schorn, T. Heimburg, 2H NMR study of cuticular wax isolated from Hordeum vulgare L. leaves: identification of amorphous and crystallinewax phases. Eur. Biophys. J. 26 (1997) 371–380.

80. L. Dassanayake, D. Kodali, S. Ueno, K. Sato, Physical properties of rice bran wax-in bulk and organogels. J. Am. Oil Chem. Soc. 86 (2009) 1163–1173.

81. C. Grant, P. Twigg, G. Bell, J.R. Lu, AFM relative stiffness measurement of the plasticising effect of a non-ionic surfactant on plant leaf wax. J. Colloid Interface Sci., 321 (2008) 360–364.

82. L. Carreto, A. Almeida, A. Fernandes, W. Vaz, Thermotropic mesomorphism of a model system for the plant epicuticular wax layer. Biophys. J. 82 (2002)530–540.

83. Y. Nibu, T. Suemori, T. Inoue, Phase bahavior of binary mixture of heptaethylene glycol decyl ether and water: formation of phase compound in solid phase. J. Colloid Interface Sci., 191 (1997) 256-263.

84. G.W. Stewart, X-ray diffraction in water: the nature of molecular association. Phys. Rev., 37 (1931) 9-16.

85. R. Aldona, Small angle neutron scattering study of two non-ionic surfactants in water micellar solutions. PRAMANA, 71 (2008) 1079-1083.

86. R. Aldona, Aggregation in heavy water micellar dilute solutions of three nonionic classic surfactants: C10E7 and C12E7 and C14E7 study by SANS method, In: Neutron and X-ray scattering in advance material research: procceedings of the international conference on neutron and X-ray scattering, 1202 (2009) 171-174.

87. F.N. Padia, M. Yaseen, B. Gore, S. Rogers, G. Bell, J.R. Lu, Influence of molecular structure on the size, shape, and nanostructure of nonionic C_nE_m surfactant micelles. J. Phys. Chem. B, 118 (2014) 179-188.

88. N.S. Murthy, W. Wang, J. Kohn, Microphase separation in copolymers of hydrophilic PEG blocks and hydrophobic tyrosine-derived segments using simultaneous SAXS/WAXS/DSC. Polymer, 51 (2010) 3978-3988.

89. X. Auvay, C. Pepitas, C. Dupuy, S. Louvet, R. Anthore, I. Rico-Lattes, A. Lattes, Small-angle X-ray diffraction study of the thermotropic and lyotropic phases of five alkyl cyclic and acyclic disaccharides: Influence of the linkage between the hydrophilic and hydrophobic moieties. Eur. Phus. J., 4 (2001) 489-504.

90. H. Takahashi, T. Hayakawa, K. Ito, M. Takata, T. Kobayashi, Small-angle and wide-angle X-ray scattering study on the bilayer structure of synthetic and bovine heart cardiolipons. J. Phys.: Conf. Ser., 247 (2010) 012021, 1-8.
91. H. Caldararu, A. Caragheorgheopol, M. Vasilescu, I. Dragutan, H. Lemmetyinen, Structure of the polar core in reverse micelles of non-ionic poly(oxyethylene) surfactants, as studied by spin probe and fluorescence probe techniques. J. Phys. Chem., 98 (1994) 5320-5331.
92. M. Vasilescu, A. Caragheorgheopol, M. Almgren, W. Brown, J. Alsins, R. Johannsson, Structure and dynamics of non-ionic polyoxyethylenic reverse micelles by time-resolved fluorescence quenching. Langmuir, 11 (1995) 2893-2998.
93. B.P. Binks, J.H. Clint, P.D.I. Fletcher, S. Rippon, S.D. Lubetkin, P.J. Mulqueen, Kinetics of Swelling of Oil-in-Water Emulsions Stabilized by Different Surfactants. Langmuir, 15 (1999) 4495–4501.
94. M. Burghardt, L. Schreiber, M. Riederer, Enhancement of the diffusion of active ingredients in barley leaf cuticular wax by monodisperse alcohol ethoxylates. J. Agric. Food Chem., 46 (1998) 1593–1602.
95. S.J Severtson, M.J Nowak, Dynamic mechanical properties and low-velocity wetting behavior of plastic crystalline states for n-alkane blends. Langmuir, 17 (2001) 4990-4996.
96. M.J. Nowak, S.J. Severtson, Dynamic mechanical spectroscopy of plastic crystalline states in n-alkane systems. J. Mat. Sci., 36 (2001) 4159 – 4166.
97. F. Lionetto, G. Coluccia, P. D'Antona, A. Maffezzoli, Gelation of waxy crude oils by ultrasonic and dynamic mechanical analysis. Rheol. Acta., 46 (2007) 601-609.
98. R. Bordes, F. Höök, Separation of bulk effects and bound mass during adsorption of surfaces probed by quartz crystal microbalance with dissipation: Insight into data interpretation. Anal. Chem., 82 (2010) 9116-9121.
99. F. Gustafson, Comparative Absorption of Cobalt-60 by Upper and Lower Epidermis of Leaves. Plant Physiol., 32 (1957) 141–142.
100. R.B. Anderson, Modifications of the Brunauer, Emmett and Teller Equation. J. Am. Chem. Soc., 70 (1946) 1727–1734.
101. J.H. de Boer, The Dynamic Character of Adsorption. Clarendon Press, Oxford, UK, 1968.
102. H. Schaefer, T.E. Redelmeier, Skin Barrier, Principles of Percutaneous Absorption. S. Karger AG. Basel, Switzerland, 1996.
103. M. Riederer, J. Schönherr, Accumulation and transport of (2,4-dichlorophenoxy) acetic acid in plant cuticles: II. Permeability of the cuticular membrane. Ecotoxicol. Environ. Saf., 9 (1985) 196–208.
104. P. Baur, H. Marzouk, J. Schönherr, H. Bauer, Mobilities of organic compounds in plant cuticles as affected by structure and molar volumes of chemicals and plant species. Planta, 199 (1995) 404–412.

ISBN 978-91-7104-576-8 (print)
ISBN 978-91-7104-575-1 (pdf)
ISSN 1653-5383

MALMÖ HÖGSKOLA
205 06 MALMÖ, SWEDEN
WWW.MAH.SE